 doi:10.20944/preprints201809.0239.v1

Article

Linear or Non Linear Modeling for ENSO Dynamics?

Marco Bianucci [1], Antonietta Capotondi[2], Riccardo Mannella [3] and Silvia Merlino[1]

[1] ISMAR-CNR, La Spezia (IT); marco.bianucci@cnr.it
[2] NOAA, Boulder, Colorado XXX
[3] Physics Department, Pisa University, Pisa (IT) 2
* Correspondence: marco.bianucci@cnr.it

Abstract: Observed ENSO statistics exhibits a non-gaussian behavior, which is indicative of the presence of nonlinear processes. In this paper we use the Recharge Oscillator model (ROM), a largely used Low-Order Model (LOM) of ENSO, as well as methodologies borrowed from the field of statistical mechanics to identify which aspects of the system may give rise to nonlinearities that are consistent with the observed ENSO statistics. In particular, we are interested in understanding whether the nonlinearities reside in the system dynamics or in the fast atmospheric forcing. Our results indicate that one important dynamical nonlinearity often introduced in the ROM cannot justify a non-gaussian system behavior, while the nonlinearity in the atmospheric forcing can instead produce a statistics similar to the observed. The implications of the non-Gaussian character of ENSO statistics for the frequency of extreme El Nino events is then examined.

Keywords: Non Hamiltonian complex systems; Fokker Planck Equation; transport coefficients; El Niño-La Niña; Lie evolution; projection approach

---

1. Non Gaussian-Non Linear features of the ENSO statistics

It is well established that some aspects of the El Niño Southern Oscillation (ENSO) have a non-Gaussian statistics, a characteristic that is indicative of some underlying nonlinear process. The histogram of the frequency of the Niño3 index (averaged sea surface temperature (SST) anomalies in the region 5°S-5°N, 150°W-90°W) shows that the likelihood of large positive SST anomalies is greater than that of negative anomalies (Fig. 1). This non-Gaussian behavior is quantified by the positive skewness : $\gamma_1 \sim 0.7$. The histogram also shows a positive kurtosis $\gamma_2 \sim 1.1$ that clearly indicates that extreme events are more likely to occur than for a normal distribution.

As previously mentioned, the non-Gaussianity of the histogram arises from non-linear contributions in the equation of motion governing the system, and it is important to understand which nonlinearities play the most relevant role in the ENSO evolution. We know that ENSO is the result of complex large-scale ocean-atmosphere interactions that also include non-linear processes, some of which arising from the ocean-atmosphere coupling itself. However, the timescale separation between the ENSO dynamics and the typical dynamics of atmospheric processes makes it possible to reduce the ENSO system to a relatively simple Low Order Model (LOM), i.e. a set of Ordinary Differential Equations (ODE). This LOM can be separated in a slow part, or "system of interest", associated with the slow evolution of oceanic variables like SST and thermocline depth, and a fast "rest of the system" that primarily includes fast atmospheric processes, e.g. the Madden-Julian Oscillation (MJO), the Westerly Wind Bursts (WWBs), etc., which are considered important in forcing ENSO. ENSO LOMs that have been extensively considered in the literature include the Recharge Oscillator Model (ROM, [1–8] among many others) and the Delayed Oscillator (DO, e.g., [9,10]). In these models ENSO events are triggered by the forcing provided by the fast atmospheric variables which are usually represented as a stochastic perturbation of the system of interest.

The simplified representation of ENSO in the LOMs provides a suitable framework for examining the impact of the system nonlinearities on the ENSO statistics. In particular, an important question

 doi:10.20944/preprints201809.0239.v1

is whether the relevant nonlinearities reside in the interaction among the variables of the system of interest (dynamical nonlinearities), or are associated with the interaction of the system of interest with the atmospheric fast forcing.

To address this issue it is worthwhile to specify better in which way statistics enter in our analysis of a deterministic system, such as ENSO. In general statistics can enter the model in two ways: considering some forcing component as stochastic (for example the fast part of the wind stress that perturbs the ocean dynamics), or assuming a deterministic motion with initial conditions distributed according to some distribution (the Gibbs idea of *ensemble*). The former approach is often used in the oceanographic field, where the dynamics is divided into a slow and a fast component, and the fast part is considered to be random (usually modeled as white noise) [11–15]. The introduction of white noise to mimic the dynamics of fast chaotic perturbing forces, reducing the deterministic dynamics to a Markov stochastic process is, of course, very common in statistical mechanics. This procedure has been formally justified by old well known works about limit theorems (e.g. [16]) and also by more recent ones, introducing some specific chaotic hypothesis (e.g. [17,18]). Actually, the mathematical theorems proved were for very special mathematical model systems, like very chaotic systems which, from a physical point of view, looked often highly idealized to be relevant for physics. In any case, once assumed to work in a stochastic framework, well known classical theorems help us to generalize this result, showing that a very broad class of stochastic dynamical systems converge (in a weak sense) to diffusion Markov processes [19]. More recent works have formally shown that, in some special cases, also a process with a finite correlation time can be reduced to a Markov stochastic process by dividing the dynamics into Markov partitions (for a review, see, e.g., the book of Dorfman[20]).

In practical cases, however, it is not usually possible to prove that the system we are interested in satisfies all the hypothesis requested by the above theorems. For example, when the fast perturbation has a multiplicative character and/or the perturbed system is non linear, it is not formally clear how to proceed to obtain this Markov partition. It is obvious that this reduction to a simple Markov process of non-linear dynamical systems perturbed by a fast chaotic perturbation that has a finite time scale is not in general possible.

In oceanography, and specifically in ENSO research, the a priori assumption of infinite time scale separation between the dynamics of the ocean and the atmosphere variables may not always be justified. Thus, in this study we shall not consider stochastic models for ENSO but just deterministic ones and we introduce a statistical description of our deterministic process by using the Gibbs idea of *ensemble*. Therefore, we assume that the state of the system is defined, at any given time, by a Probability Density Function (PDF) on the whole phase space spanned by the variables of the system.

2. The dynamics of the components of the ENSO

The El Niño Southern Oscillation, also known as ENSO, is a periodic fluctuation of the SST (El Niño) and the see level pressure (Southern Oscillation) across the equatorial Pacific ocean. The fluctuations arise over a normal condition of strong SST gradient between the east (cold tongue) and the west (warm pool) equatorial Pacific ocean. ENSO is a complicated, not yet fully understood, coupled ocean-atmosphere phenomenon in which basin-wide changes in sea surface temperatures, trade winds, and atmospheric convection are intimately related. However, the particular ocean and atmosphere conditions that generate, and in some way also define, the El Niño/La Niña events, allow the representation of the key ocean-atmospheric feedbacks responsible for this complex phenomenon in a simplified fashion.

The upper layer of the tropical Pacific ocean, responsible for the energy and momentum exchange with the atmosphere, is a very long strip of water with a meridional width of a few hundred kilometers, a zonal extension of about 10.000 km, and an average depth of about 120m, as defined by the depth of the thermocline. The water in this strip flows over the deeper and colder ocean, from the south America coasts to the warm Asian coasts, mainly driven by the easterly trade-winds and "trapped" in the convergence ocean zone, around the equatorial latitude, ultimately due to the Coriolis effect.

Preprints (www.preprints.org) | NOT PEER-REVIEWED | Posted: 13 September 2018 doi:10.20944/preprints201809.0239.v1

This motion accumulates warm water in the western Pacific ocean and because of the closed eastern boundary it forces the cold and deep water to rise up in the eastern Pacific to compensate the surface water moving westward. This process generates the strong SST gradient between the two sides of the basin, which, in normal conditions, is in equilibrium with the easterly trade winds.

During an El Niño (La Niña) event this SST gradient from east to west is reduced (increased): we consider that a El Niño (La Niña) event is occurring when the SST anomaly on the east equatorial pacific is greater (lesser) than 0.5 (-0.5) degrees Celsius with respect to the average value. The SST anomalies are related to the thermocline depth anomalies. Thus the key quantities that characterize ENSO in the equatorial Pacific ocean are the SST anomaly (T) in the eastern part of the domain, usually described in terms of the Niño3 index (average SST in the area 5N-5S, 150W-90W) , and the zonal average of the anomaly of the thermocline depth (h).

Exploiting these very peculiar physical conditions of the equatorial surface layer of the Pacific ocean and from a two-boxes (east and west side, respectively), two strips (equatorial and off equatorial, respectively) approximations of the shallow water Navier Stokes (NS) equations applied to the tropical Pacific ocean, Jin obtained the following very simple system of *linear* equations for the Pacific Equatorial thermocline depth anomaly [1,2]:

$$\dot{h}_W = -r\, h_W - \alpha\, \tau_s \tag{1a}$$

$$h_E - h_W = \tau_s \tag{1b}$$

where τ_s is the zonally integrated wind stress anomaly, the subscript W (E) means that the variables refer to the west (east) side of the basin, the friction term r collectively represents the damping of the upper ocean system through mixing and the equatorial energy loss to the boundary layer currents at the east and west sides of the ocean basin and it is set in the range $6.3\,\text{month} \lesssim r^{-1} \lesssim 8.0\,\text{month}$ [1,2]. Eq. (1b) describes the zonal tilt of the thermocline which is in balance with the equatorial zonal wind stress forcing on interannual time scales (e.g. [1,21]). The Kelvin and Rossby waves, that accomplish the adjustment processes, are filtered out, in this picture, because the timescale of the mode retained in this approximation is much longer than the basin crossing time of theses waves. If one assumes that for a given steady wind stress forcing, the zonal mean thermocline anomaly of this linear system is about zero at the equilibrium state, that is, $h_E + h_W = 0$ (at equilibrium), then from Eq. (1) one finds that α shall be about half of r.

Refs. [1,2] provide a physical basis for the simple linear relationships in Eq. (1), in the long wave, two strip approximation.

Notice that if the wind stress τ_s was a fast forcing completely independent of the dynamics of the thermocline depth anomaly, Eq. (1) would give rise to a very simple relaxation process with relaxation time given by $1/r$, that, of course, is not what happens in reality. In fact, as we shall see below, the wind dynamics has a slow part that is strongly correlated with the dynamics of h via a direct linear relationship with the other ENSO variable: the SST anomaly T.

A *linear* ODE for the thermodynamics relationship between the variation of the anomalous SST and the thermocline depth is proposed in Refs. [1,2,22,23] and related subsequent works:

$$\dot{T}_E = -c\, T_E + \gamma\, h_E + \delta_S \tau_{s,E}. \tag{2}$$

where the first term on the right-hand side is a damping process with a collective damping rate c. The second term describes the influence on T_E of the thermocline displacement and δ_S is the Ekman pumping coefficient of the vertical advective feedback processes due to the wind stress averaged over the domain, that actually can be considered vanishing (see [1,22,23] for details): $\delta_S = 0$.

Using Eq. (1b) we can rewrite Eq. (2) as:

$$\dot{T}_E = -c\, T_E + \gamma\, h_W + \gamma\, \tau_s. \tag{3}$$

Preprints (www.preprints.org) | NOT PEER-REVIEWED | Posted: 13 September 2018 doi:10.20944/preprints201809.0239.v1

The above equation relates the dynamics of T_E to that of h_W. However, as we have already observed, also the dynamics of h_W, given in Eq. (1), depends on the values of the T_E variable. This dependence is due to the fact that the wind stress τ_s is strongly influenced by the zonal SST gradient. In effect, in most of the works on the ROM [22,23] and on the DO [9] it is explicitly assumed that the following *linear* relationship holds true:

$$\tau_s = b\, T_E + g(t), \tag{4}$$

where $g(t)$ is a fast chaotic fluctuating function of time. The above equation means that the slow component of the wind stress and the slow component of T_E are proportional to each other. Fig. 1 of the paper [24] supports this assumption, and we further validate this hypothesis by analyzing the NOAA data [25] as detailed in Appendix A, where the wind stress anomaly τ_s is divided in a slow ($\tau_{s,slow}$) and fast ($\tau_{s,fast}$) components. The $\tau_{s,slow}$ data are obtained from the one year average of τ_s data, while $\tau_{s,fast} \equiv \tau_s - \tau_{s,slow}$ can be identified with $g(t)$ of (4).

Exploiting Eq. (4), from Eqs. (1b) and (3) we obtain the well-known *linear* ROM:

$$\begin{aligned} \dot{h}_W &= -r h_W - \alpha b T_E - \alpha g(t) \\ \dot{T}_E &= \gamma h_W - \lambda\, T_E + \gamma g(t), \end{aligned} \tag{5}$$

with $\lambda \equiv c - \gamma b$.

Considering that α is quite smaller than γ [1,2], we can disregard the forcing term $-\alpha g(t)$ in the first equation of system (5) and finally, we are led to the following simplified *linear* ROM:

$$\begin{aligned} \dot{h}_W &= -r h_W - \alpha b T_E \\ \dot{T}_E &= \gamma h_W - \lambda\, T_E + g(t) \end{aligned} \tag{6}$$

where we have included the constant γ in the definition of the fast part $g(t)$ of the wind stress τ_s. The result of Eq. (6) is really remarkable because it is a very simple, but still informative, description of a complex large scale ocean/atmosphere process. We can consider it on the same footing as the Onsager linear regression principle, chemical reaction rate models [26] and other linear results of standard thermodynamics and statistical mechanics, that arise as large time and space scale phenomena from a underlying complex fast and chaotic dynamics.

Notice that the "internal" dynamics (i.e., for $g(t) = 0$) of the ROM of Eq. (6) is linear, and this is due to the linear relationship between h_E and T_E of Eq. (2). However, nonlinearities may be present and their influence should be considered. In fact, in Ref. [9] it is argued that a *nonlinear* cubic relationship between the anomalous subsurface temperature T_{sub} and the thermocline depth anomaly should be taken into account:

$$T_{sub} = a\, h_E - e^*\, h_E^3 + O(h_E^5), \tag{7}$$

where the values for the coefficients a and e have been roughly estimated in [9] as $a \sim 0.14\,^\circ\mathrm{C\,m^{-1}}$ and $e^* \sim 3 \times 10^{-5}\,^\circ\mathrm{C\,m^{-2}}$. From this nonlinear relation, a small cubic term in h_E would enter also in Eq. (2) [9]. Given the values of the a and e^* parameters, the cubic term should play some role for $h_E \geq \pm 2\sigma_{h_E}$ (σ_{h_E} is the standard deviation of h_E that is a little over 10 m [27]), reaching the same value of the linear term for $h_E = \sqrt{a/e^*} = 36$ m (about $3\sigma_{h_E}$). Using these arguments, in [28] it has been already shown that a non linear ROM, linearly interacting with the atmosphere, has a non normal stationary PDF. However, as we can see in Ref. [24], Figure 5, both observations and numerical results show that the relationship between T_{sub} and h is mainly linear, with a small dispersion of the data around the linear fit and with a coefficient that is close to one when the quantities are normalized by the standard deviation of the quantities from observations. In this figure the values for h_E range from $\pm 4\sigma_{h_E}$, thus it follows that in Eq. (7) the coefficient e^* of the nonlinear term must be really small,

Preprints (www.preprints.org) | NOT PEER-REVIEWED | Posted: 13 September 2018 doi:10.20944/preprints201809.0239.v1

smaller than the value estimated in [9]. Despite that, for now we take into account this small nonlinear term, that only comes into play for very strong ENSO.

Thus we consider the following non linear ROM:

$$\begin{aligned} \dot{h}_W &= -rh_W - \alpha b T_E \\ \dot{T}_E &= \gamma U'(h_W) - \lambda\, T_E + g(t), \end{aligned} \tag{8}$$

in which

$$U(h_W) = h_W^2/2 + \kappa h_W^4/4 + O(h_W^6) \tag{9}$$

where κ is a small parameter order $10^{-4}\,\mathrm{m}^{-4}$ and for a generic function $f(x)$ we have defined $f'(x) = df(x)/dx$. To verify if the nonlinearity due to a non vanishing value of κ can justify, at least to some extent, the non Gaussian features of the observed Niño3 index shown in Fig. 1, we try to find the stationary PDF that can be derived from Eq. (8), considering $g(t)$ as an *additive* fast fluctuating forcing. For that, we change variables: $v \equiv -rh_W - \alpha b T_E$, $x = h_W$. Eq. (8) becomes:

$$\begin{aligned} \dot{x} &= v \\ \dot{v} &= -\alpha b\gamma U'(x) - (r+\lambda)\, v - \lambda r\, x - \alpha b\, g(t). \end{aligned} \tag{10}$$

If $g(t)$ is assumed to be a white noise with a correlation function $\langle g(0)g(t)\rangle = 2d\delta(t)$, Eq. (10) describes the dynamics of a particle with coordinate x, velocity v, in a "almost" harmonic potential given by

$$V(x) = \alpha b\gamma U(x) + \lambda r\frac{x^2}{2} \simeq (\lambda r + \alpha b\gamma)\frac{x^2}{2} + \alpha b\gamma\,\kappa\frac{x^4}{4} \tag{11}$$

and interacting with a thermal bath with friction $r+\lambda$ and "temperature" $\Theta = \alpha^2 b^2 d/(r+\lambda)$. It is well known that the stationary PDF for such a system is the "Canonical" one:

$$\rho_s(x,v) = Z\, e^{-\frac{H(x,v)}{\Theta}}, \tag{12}$$

where Z is the normalization constant and $H(x,v) \equiv V(x) + \frac{v^2}{2}$ is the Hamiltonian. Thus, Θ is the variance of the "velocity" variable v: $\Theta = \langle v^2\rangle_s \equiv \sigma_v^2$. As for the x $(= h_W)$ variable, we notice that, given the small value of the κ parameter, the non harmonic term $\alpha b\gamma\,\kappa\, x^4/4$ in the potential $V(x)$ of Eq. (11) gives a negligible contribution to the variance, thus we also have $\Theta \simeq (\lambda r + \alpha b\gamma)\langle x^2\rangle_s \equiv (\lambda r + \alpha b\gamma)\sigma_x^2$. Therefore the stationary PDF of Eq (12) is very well approximated by a Gaussian function till $x = h_W$ far exceeds 2 standard deviations, when, in any case any non Gaussian feature could not really emerge because of the low probability. Thus we are led to the conclusion that the observed non Gaussian properties of the ENSO statistics are not due to the possibly non linear interaction between the internal ROM variables.

Notice that if we consider the external forcing $g(t)$ as a correlated noise (i.e., not white) or as a weak deterministic chaotic perturbation, using a Zwanzig'-like projection approach in the perturbation version of [29–31] we obtain in any case a stationary PDF for the ROM variables that is similar to the one in Eq. (12), apart from some small changes in the parameter Θ and in the coefficients of the potential $V(x)$. Thus also in these non Markovian cases the same argument of the previous white noise case applies: the non Gaussian features of the PDF would be negligible and not as pronounced as seen in observations.

So far we have shown that analyzing the relations between the dynamics of h_W and T_E, it is hard to find nonlinearities strong enough to justify the non Gaussian behavior of the ENSO statistics. Thus, from now on we shall assume that the non harmonic term in the potential $U(h_W)$ of Eq. (9) can

Preprints (www.preprints.org) | NOT PEER-REVIEWED | Posted: 13 September 2018 doi:10.20944/preprints201809.0239.v1

be neglected. Namely, we return to the linear ROM of Eq. (6) and attempt to justify the observed nonlinearities focusing on the interaction of the slow components of the ROM of Eq. (6) with $g(t)$.

It is worthwhile remarking that a recent study [32] has highlighted the importance of the nonlinear advective terms in the upper-ocean temperature equations as a source of ENSO nonlinearities and the resulting non-Gaussianity of eastern Pacific SST anomalies. These nonlinear advective terms, which have been collectively termed Nonlinear Dynamical Heating (NDH) are primarily controlled by the anomalies of the zonal advection term ($u'\partial_x T'$, see [32] for the nomenclature). However, the asymmetric influence of the nonlinear zonal advection term upon warm and cold ENSO events may be linked to the distinctive multiplicative character of the anomalous wind forcing of ENSO, which is stronger for positive than negative anomalies. Nonlinearities in the surface forcing and their influence on the SST statistics are described in the next section.

Before doing that, however, we simplify a little Eq. (6) in the following way:

$$\begin{aligned} \dot{h} &= -\omega\, T_E \\ \dot{T}_E &= \omega\, h - \lambda\, T_E + g(t), \end{aligned} \tag{13}$$

where $h \equiv (h_W + h_E)/2$ is the zonally averaged thermocline depth anomaly (directly related to the anomalous heat accumulated in the Equatorial Pacific ocean), a choice justified by the arguments and results of [3], shortly summarized hereafter. First, Eq. (1b) implies that the tilt of the thermocline reacts almost instantaneously to wind stress, but it is more realistic to assume that the adjustment of the thermocline depth takes a finite time, approximately the time it takes for a Kelvin wave to propagate from the western central Pacific to the east. Thus Eq. (1b) should be replaced by

$$\dot{h}_E = -\gamma_h(h_E - h_W - \tau_s).$$

Second, repeating the same steps that lead us from Eq. (1b) to Eq. (6), we get an unperturbed ROM given by three differential equations that better represents the ENSO dynamics, leading to a better agreement among the parameter of the model and observations. Finally, studying in detail the feature of this linear 3-degrees of freedom system, we see that one eigenstate has a fast decay time (shorter than one month), thus, the dynamics is attracted toward a 2-dimensional slow manifold, well represented by the reduced ROM of Eq. (13).

Suitable values for ω and λ (the "friction" coefficient), can be obtained by using phenomenological considerations when deriving the ROM from building block equations, and/or directly from a fit to observations (see [3]). In literature, we find different values that range from $2\pi/48\,\text{month}^{-1}$ to $2\pi/36\,\text{month}^{-1}$ for ω and from $1/12\,\text{month}^{-1}$ to $1/6\,\text{month}^{-1}$ for λ. We shall see in the following that we can shrink these ranges.

3. The multiplicative nature of the forcing

In some recent works it has been shown that to account for the instability of the dynamics, the skewness and the tail of the observed stationary PDF of the ENSO, the perturbation forcing $g(t)$ of the ROM cannot be simply additive, but a multiplicative term, directly correlated with the additive one, should also be considered [5,6,8], leading to a stochastic perturbation of the form:

$$g(t) = \epsilon(1 + \beta T_E)\xi(t), \tag{14}$$

where $\xi(t)$ is a fast chaotic fluctuating term and ϵ is a parameter that controls the strength of the interaction. Many facts support the hypothesis given by Eq. (14):

- the multiplicative nature of the ENSO forcing provided by the Madden-Julian oscillation (MJO) and its higher frequency tail [33,34, and references therein];
- multiplicative fast forcings typically emerges from the general perturbation approaches to large scale ocean dynamics [35,36];

Preprints (www.preprints.org) | NOT PEER-REVIEWED | Posted: 13 September 2018 doi:10.20944/preprints201809.0239.v1

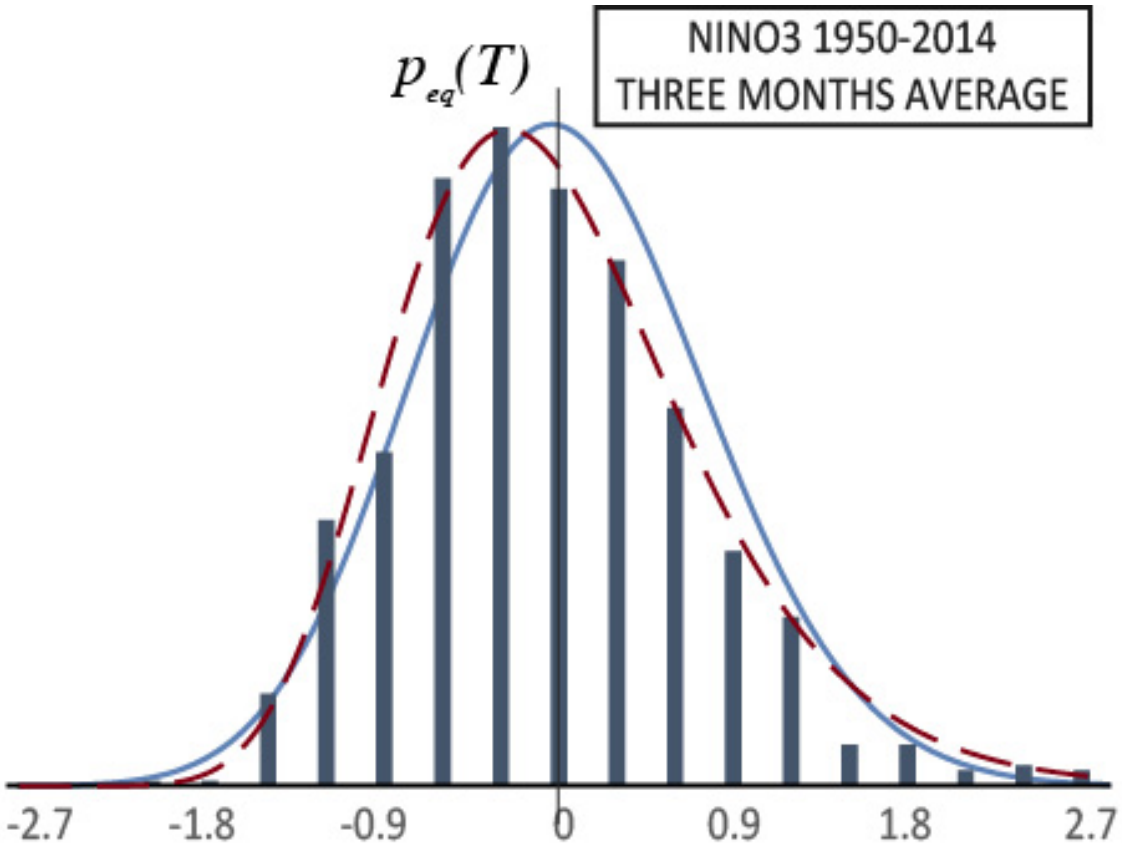

Figure 1. Histogram of the frequency for the three months average NINO3 data from NOAA [39]. Dashed line is the best fit of the stationary PDF found in [8] (strongly skewed and with a heavy tail), solid blue line is a normal distribution with same average and variance of the observation data.

- considering the nonlinear nature of the heat budget equation for the surface mixed layer [37] we get multiplicative fast fluctuations in both the net surface/subsurface heat flux and the advective contributions [7,32,35,36].

Concerning the last point, we again notice that the equatorial Pacific zonal subsurface NDH $u'\partial_x T'$, that plays a role in the asymmetry of the El Niño-La Niña events [32], may be linked to the multiplicative term $\epsilon\beta T_E\xi(t)$ of Eq. (14), assuming that $\xi(t)$ and T_E are directly related to u' and $\partial_x T'$, respectively.

Thus, inserting Eq. (14) in the ROM of Eq. (13), we get:

$$\begin{aligned} \dot{h} &= -\omega\, T_E \\ \dot{T}_E &= \omega\, h - \lambda\, T_E + \epsilon(1+\beta T_E)\xi(t), \end{aligned} \tag{15}$$

that is the final model we shall take into account hereafter.

When $\xi(t)$ is a white noise, the term $(1+\beta T_E)\xi(t)$ is often named Correlated-Additive-Multiplicative (CAM) noise [11–13], but we shall extend this notation also to deterministic (i.e., not stochastic) processes, saying that $(1+\beta T_E)\xi(t)$ is a CAM forcing. In Section 5, starting from observations, we shall use a statistical inference method for diffusion processes with nonlinear drift to estimate the effective contribution of the CAM forcing with respect to a more simple additive fast forcing.

Preprints (www.preprints.org) | NOT PEER-REVIEWED | Posted: 13 September 2018 doi:10.20944/preprints201809.0239.v1

In general, it is reasonable that at least a part of the additive forcing should not be correlated with the multiplicative one, i.e., that there are different independent fast chaotic forcing that can be collected as an independent additive contribution, uncorrelated to the previous one, considered above:

$$g(t) = f(t) + (1 + \beta T_E)\xi(t), \tag{16}$$

where $f(t)$ is uncorrelated with $\xi(t)$. However, for the sake of simplicity, we do not consider this possibility here. This more general ROM will be examined in a subsequent paper.

We want to stress again that we do not make the assumption that the forcing term $\xi(t)$ of Eq. (15) has a stochastic nature. $\xi(t)$ is a deterministic "chaotic" forcing, and statistics is introduced by using the Gibbs concept of *ensemble* (our PDF).

4. The Fokker Planck Equation guiding the statistics of the ROM

The ROM of Eq. (15) must be validated by observations of the ENSO, namely we must use some data analysis approach to infer the values of the coefficients of the ROM of Eq. (15). Due to the multiplicative character of the perturbation, the system is not linear thus, strictly speaking, well consolidated approaches based on the Gaussian properties of the data dispersion, such as the LIM, cannot be used in this case. However, as it will be shown in the next Section, if we observe only, or if we are interested only in the first (the mean) and the second (the variance) moments, then the system of Eq. (15) looks like linear, with eigenvalues that are weakly renormalized by the β parameter and a constant forcing that depends linearly on β. Of course, replacing the non linear ROM of Eq. (15) with a linear one, all the informations concerning large deviations from the averages will be lost.

To be really in a position to distinguish, in the model of Eq. (15), between the dynamics of the ENSO variables of interest (h, T_E), and that of the "rest of the system", mimicked by the collective variable $\xi(t)$, it is implicitly assumed that there is a time scale separation and/or a weak interaction between these two sub systems. It is a fact that the dynamics of the atmosphere forcing triggering the ENSO, that is represented by the term proportional to the ϵ parameter in Eq. (15), has a time scale that is shorter than the time scale of the average dynamics of the ENSO. Thus, we can say that the autocorrelation time τ of $\xi(t)$ is smaller than the period and relaxation time of the unperturbed ROM, given by $1/\sqrt{\omega^2 - \lambda^2/4}$ and $2/\lambda$, respectively. Notice that "shorter" does not necessarily mean "extremely shorter", but, if this is the case, we can approximate $\xi(t)$ by a white noise [17–20], with $\langle \xi(0)\xi(t)\rangle = 2\langle \xi^2\rangle \tau \delta(t)$. It is a well known result that if $\xi(t)$ is replaced with a white noise, Eq. (15) becomes equivalent to the following Fokker Planck Equation (FPE) for the Probability Density Function (PDF) $\sigma(h, T; t)$ of the ROM variables (we shall use the Stratonovich integration rule for white noise dynamics [40], hereafter for the sake of simplicity we shall use T for T_E and $\partial_t \equiv \partial/\partial t$, $\partial_h \equiv \partial/\partial h$ and $\partial_T \equiv \partial/\partial T$):

$$\begin{aligned}
\partial_t \sigma(h, T; t) =& \{\omega\, \partial_h T - \omega\, \partial_T h + \lambda\ \partial_T T + D\, \beta\, \partial_T (1 + \beta\, T) \\
&+ \partial_T\, D\, (1 + \beta T)^2 \partial_T\} \sigma(h, T; t) \\
=& \{\omega\, \partial_h T - \omega\, \partial_T h + \lambda\ \partial_T T - D\, \beta\, \partial_T (1 + \beta\, T) \\
&+ \partial_T^2\, D\, (1 + \beta T)^2\} \sigma(h, T; t)
\end{aligned} \tag{17}$$

where $D \equiv \epsilon^2 \langle \xi^2 \rangle \tau$ is the "standard" diffusion coefficient.

In the case where the time scale separation between the unperturbed ROM and the fast forcing is not so extreme, as we have already stressed we cannot approximate the deterministic forcing $\xi(t)$ with a white noise, and we have to work with *ensembles* (i.e., PDF) of which the time evolution is guided by the Liouvillian corresponding to the equation of motion of the perturbed ROM of Eq. (15). Starting from the Liouville equation, assuming weak perturbation of the ROM (small ϵ values), and using a projection perturbation approach, it is thus possible to derive an effective FPE that well approximates

Preprints (www.preprints.org) | NOT PEER-REVIEWED | Posted: 13 September 2018 doi:10.20944/preprints201809.0239.v1

the dynamics of the PDF [8] (see also Appendix B for a short summary of this projection procedure, adapted to the present case of Eq. (15)):

$$\begin{aligned}\partial_t \sigma(h,T;t) = &\{\omega\,\partial_h T - \omega\,\partial_T h \\ &+ (\lambda + D\,\beta^2)\,\partial_T T + D\,\beta\,\partial_T \\ &+ \partial_T A(h,T)\,\partial_T + \partial_T B(h,T)\,\partial_h\}\sigma(h,T;t),\end{aligned} \tag{18}$$

where the decay time τ of the auto-correlation function of ξ is defined in the following way: if $\varphi(t) \equiv \langle \xi(t)\,\xi(0)\rangle / \langle \xi^2 \rangle$ is the normalized autocorrelation function of ξ, then $\tau \equiv \int_0^\infty \varphi(t)\mathrm{d}t$. As in [8], the diffusion functions $A(h,T)$ and $B(h,T)$ are second order polynomials of the ROM variables (h,T):

$$\begin{aligned}A(h,T) =& A_0 + \beta A_1\,h + \beta A_2\,T \\ &+ \beta^2 A_3\,hT + \beta^2 A_4\,T^2 \\ B(h,T) =& B_0 + \beta B_1\,h + \beta B_2\,T \\ &+ \beta^2 B_3\,hT + \beta^2 B_4\,T^2.\end{aligned} \tag{19}$$

As it is shown in Appendix B, the A_i and B_i coefficients are proportional to ϵ^2, do not depend on the β parameter and are linear combinations of the Fourier transform of the function $\varphi(t)$, evaluated at the frequencies 2Ω and $\Omega - i\lambda/2$, where $\Omega \equiv \sqrt{\omega^2 - \lambda^2/4}$ is the effective frequency of the unperturbed ROM.

From the FPE it is possible to get all the relevant statistical information about the ENSO variables, including the T moments and the stationary PDF. From a formal point of view, it is worthwhile mentioning the fact that the FPE in Eq. (18) is a second order Partial Differential Equation (PDE) with discriminant [41] equal to $B(h,T)^2/2 \geq 0$, thus, for non vanishing $B(h,T)$, this PDE is hyperbolic, and not parabolic as the FPE of Eq. (17) stemming from "true" stochastic Markovian processes. The diffusion coefficient $B(h,T)$ is a signature of the finite (i.e. "non infinite") time scale separation between the dynamics of the system of interest and that of the booster.

5. Inference of the statistical features of the ROM from observations

5.1. Linear equation of motion for the first two moments of the ROM and the white noise approximation

Using the FPE of Eqs. (18)-(19), it is easy to obtain a set of closed equations of motion for the first n-th moments of the ROM. For the moments up to the second ones we get:

$$\begin{aligned}\langle \dot{h} \rangle &= -\omega\,\langle T \rangle \\ \langle \dot{T} \rangle &= (\omega + \beta^2 A_3)\,\langle h \rangle - (\lambda - \beta^2 A_4)\,\langle T \rangle + \beta A_0\end{aligned} \tag{20a}$$

$$\begin{aligned}\langle \dot{h^2} \rangle &= -2\omega\,\langle hT \rangle \\ \langle h\dot{T} \rangle &= (\omega + \beta^2 A_3)\,\langle h^2 \rangle \\ &\quad - (\lambda - \beta^2 D)\,\langle hT \rangle - (\omega - \beta^2 B_4)\,\langle T^2 \rangle \\ &\quad + \beta\,(D + A_0 - A_4)\,\langle h \rangle - \beta B_2\,\langle T \rangle + B_0 \\ \langle \dot{T^2} \rangle &= 2(\omega + 2\beta^2 A_3)\langle hT \rangle - 2\left(\lambda - \beta^2\,2A_4\right)\langle T^2 \rangle \\ &\quad + 2\beta\,(2A_0 + A_4)\,\langle T \rangle + 2\beta A_3 \langle h \rangle + 2A_0,\end{aligned} \tag{20b}$$

Preprints (www.preprints.org) | NOT PEER-REVIEWED | Posted: 13 September 2018 doi:10.20944/preprints201809.0239.v1

from which (hereafter the subscript "s" stands for "stationary")

$$\begin{aligned}\langle T^2\rangle_s =& \frac{A_0}{\lambda - 2\,\beta^2\,A_4}\left(1 - \frac{\beta^2\,A_3}{\beta^2\,A_3 + \omega}\right)\\ \approx& \frac{A_0}{\lambda}\left[1 + \beta^2\left(2\frac{A_4}{\lambda} - \frac{A_3}{\omega}\right)\right] + O(\epsilon^6) \approx \frac{A_0}{\lambda} + O(\epsilon^4)\end{aligned} \tag{21}$$

Thus, the width of the stationary PDF can be considered independent of β.

Eq. (20a) is equivalent to the equation of motion of a linear dissipative oscillator, with bare frequency $\sqrt{\omega^2 + \beta^2 A_3}$ and friction coefficient $(\lambda - \beta^2 A_4)$, perturbed by the constant force $\beta\,A_0$. The weak perturbation assumption (small ϵ) and the fact that $\beta \sim 0.2$ imply that $\omega + \beta^2 A_3 \sim \omega$ and $(\lambda - \beta^2 A_4) \sim \lambda$. Thus, the equation of motion of the first moment (Eq. (20a)) is very similar to that of the unperturbed ($\epsilon = 0$) ROM (apart from the constant forcing βA_0 that can be disregarded, as we will show shortly). This fact is really important because from a physical point of view it gives a sound meaning to the definition of unperturbed ROM of Eq. (13): it is the dynamical system that corresponds to the "slow" part of the ENSO dynamics.

Concerning the constant force βA_0 appearing in Eq. (20a), it is not really measurable, in fact it is an "artifact" of the final approximation that, from the ROM of Eq. (6), leads to Eq. (15). This is clear from the fact that this constant forcing yields a non vanishing average stationary value for the thermocline depth anomaly: $\langle h\rangle_s \sim -\beta A_0/\omega$. To cure this flaw we should replace h with $h - \beta\,A_0/\omega$ in Eq. (15). However, because we shall focus our attention on T, we will leave the ROM unchanged.

Concerning the equations of motion of the second moments (Eq. (20b)), we see that they weakly depend on the B diffusion coefficient. Moreover, using the relationships of Eqs. (B9), (B13) and (B14), we have that they mainly depend on β and A_0, thus, the dynamics of the second moments should not depend too much on the time scale separation between the average ROM dynamics and that of the fast forcing ξ. Estimates of the time scale $1/\lambda$ are in the range of 6-12 months. Assuming an exponential decay of the autocorrelation function of ξ, i.e. $\varphi(t) = \exp(-t/\tau)$, we can verify that for τ up to ~ 3 month the transport coefficient A has the same structure it has in the limit of very large time scale separation ($\tau \to 0$), namely $A(T) \sim A_0\,(1 + \beta T)^2$ (see Fig. 2) and, as it is shown in Fig. 3, the dynamics of the second moments is almost independent of τ. The results of this section allow us to get two main important conclusions:

1. analyzing only the first and second moments/cumulants/cross-correlation functions of the observations data we cannot identify/detect the (possible) non linearity due to the interaction with the atmosphere, in the ENSO system;
2. comparing the first and second moments/cumulants/cross-correlation functions we obtain from the FPE of Eq. (18) with observations, it would be really hard to determine how small is the time scale τ of decaying of the correlation function of the effective noise perturbing the ROM. On the other hand, as it has been shown in [8], also for $\tau \to 0$ the FPE of Eq. (18) well accounts for the non Gaussianity of the ENSO statistics. Thus, for the sake of simplicity, from now on, we shall use the FPE of Eq. (17) that is the white noise limit of Eq. (18), even if we are aware of the fact that the time scale separation between the dynamics of the averaged ROM and that of the fast atmosphere is not so "extreme".

In the next sub-section we shall analyze the point 1 in detail.

5.2. The covariance matrix of the ROM and the comparison with the ENSO data

Given the results of the previous sub-section, we assume that to describe the statistics of the ENSO we can use the simplified FPE of Eq. (17), instead of the more general Eq. (18). This FPE must be validated with data from observations.

Preprints (www.preprints.org) | NOT PEER-REVIEWED | Posted: 13 September 2018 doi:10.20944/preprints201809.0239.v1

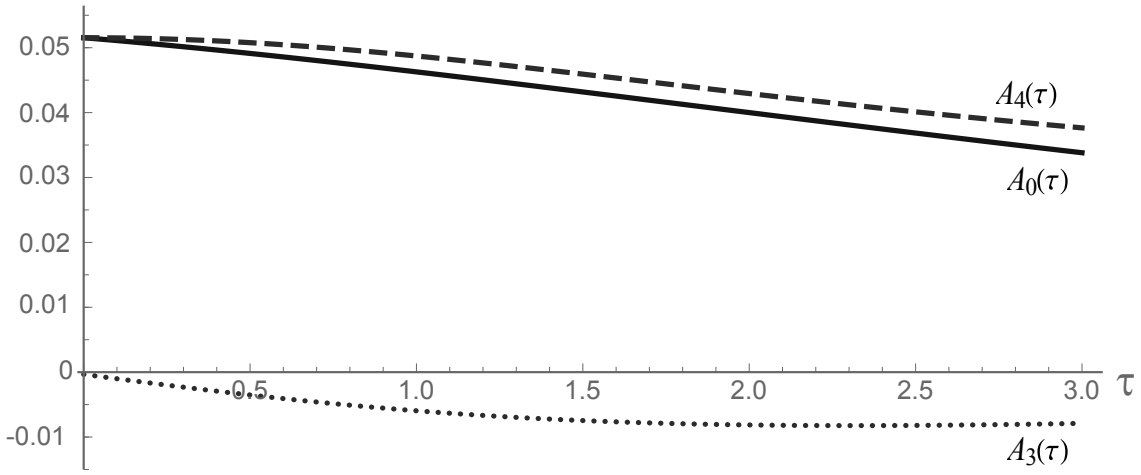

Figure 2. The values of the coefficients A_0, A_4 and A_3 vs τ for $\varphi(t) = \exp(-t/\tau)$ for $1/\lambda = 12$ month. In the shown range 0 month $\leq \tau \leq 3$ month, $A_4 \sim A_0$ and $A_3 \sim 0$. We recall that $A_2 = A_4 + A_0$ and that $A_1 = A_3$. Thus $A \sim A_0(1+\beta T)^2$, which must be compared to $A = D(1+\beta T)^2$ that holds true in the limit of a very large time scale separation between the dynamics of the ROM and that of the booster (see text for details).

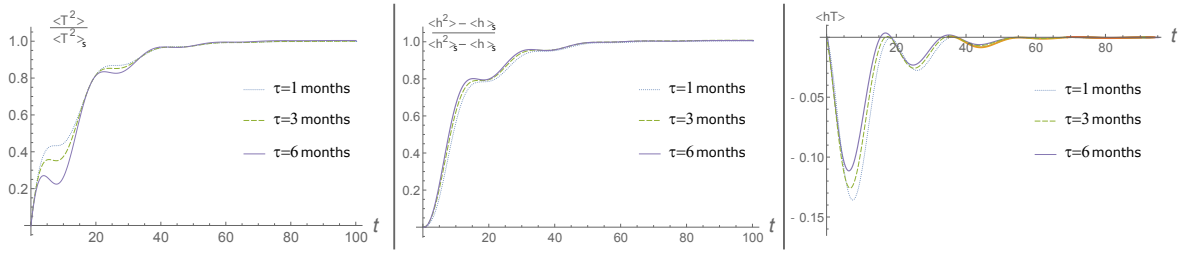

Figure 3. Evolution of the variance of T (left), h (center) and of the cross-correlation between T and h, obtained from Eq. (20b) with the A_i and B_i coefficients given by Eqs. (B6)-(B13), in the case where $1/\lambda = 12$ month and $\varphi(t) = \exp(-t/\tau)$, for different values of τ. Solid line: $\tau = 6$ month; dashed line: $\tau = 3$ month; dotted line: $\tau = 1$ month. Curves for different τ values are very similar.

Preprints (www.preprints.org) | NOT PEER-REVIEWED | Posted: 13 September 2018 doi:10.20944/preprints201809.0239.v1

To this end, we write again the first equations for the time evolution of the first two moments, using the FPE Eq. (17) (we also use the shift $h \to h + \beta D/\omega$ to ensure that the mean value of the thermocline depth anomaly is zero):

$$\begin{aligned} \langle \dot{h} \rangle &= -\omega \langle T \rangle \\ \langle \dot{T} \rangle &= \omega \langle h \rangle - (\lambda - \beta^2 D) \langle T \rangle \sim \omega \langle h \rangle - \lambda \langle T \rangle \end{aligned} \tag{22a}$$

$$\begin{aligned} \langle \dot{h^2} \rangle &= -2\omega \langle hT \rangle \\ \langle h\dot{T} \rangle &= \omega \langle h^2 \rangle - (\lambda - \beta^2 D) \langle hT \rangle - \omega \langle T^2 \rangle \\ &\sim \omega \langle h^2 \rangle - \lambda \langle hT \rangle - \omega \langle T^2 \rangle \\ \langle \dot{T^2} \rangle &= 2\omega \langle hT \rangle - 2(\lambda - 2\beta^2 D) \langle T^2 \rangle + 4\beta D \langle T \rangle + 2D \\ &\sim 2\omega \langle hT \rangle - 2\lambda \langle T^2 \rangle + 4\beta D \langle T \rangle + 2D. \end{aligned} \tag{22b}$$

For sake of simplicity, in the above equations we have explicitly made the approximation of neglecting the terms proportional to $\beta^2 D$, assuming that $\epsilon \ll 1$ and $\beta \ll 1$. The validity of this assumption will be shown later. In any case, these approximations could be weakened without affecting the derivation below. From the above equations we get the following stationary first and second moments:

$$\begin{aligned} \langle h \rangle_s &= \langle T \rangle_s = 0 \\ \langle h^2 \rangle_s &= \langle T^2 \rangle_s \sim \frac{D}{\lambda}. \end{aligned} \tag{23}$$

The values of the ratio D/λ can be obtained from the observations with a very good accuracy. According to Eq. (23), D/λ can be inferred from the variance $\sigma^2 = \langle T^2 \rangle_s$ of the Niño3 time series, leading to values of D/λ between 0.60 and 0.66 (we recall that $D \equiv \epsilon^2 \langle \xi^2 \rangle \tau$ is the "standard" diffusion coefficient). For the other coefficients in the FPE of Eq. (17), we focus our attention on the elements of the covariance matrix $\langle x(t) y(0) \rangle_s$, where "$x$" and "$y$" can be either h or T. We note that by definition we have:

$$\langle x(t) y(0) \rangle_s = \langle \left(e^{\mathcal{L}^+_{FPE} t} x \right) \, y \rangle_s \tag{24}$$

where $\mathcal{L}^+_{FPE}$ is the adjoint of the Liouvillian defined by the FPE of Eq. (17). Thus the evolution $(e^{\mathcal{L}^+_{FPE} t} h)$ and $(e^{\mathcal{L}^+_{FPE} t} T)$ are solutions of the differential equations for the lowest order moments of Eq. (22a). Because Eq. (22a) is linear, the solutions will be linear combinations of h and T:

$$\begin{aligned} \left(e^{\mathcal{L}^+_{FPE} t} h \right) &= a_{h,h}(t)\, h + a_{h,T}(t)\, T \\ \left(e^{\mathcal{L}^+_{FPE} t} T \right) &= a_{T,h}(t)\, h + a_{T,T}(t)\, T \end{aligned} \tag{25}$$

where

$$\begin{aligned} a_{h,h}(t) &= e^{-\frac{\lambda}{2} u} \left[\cos(\Omega\, u) + \frac{\lambda}{2} \frac{\sin(\Omega\, u)}{\Omega} \right] \\ a_{h,T}(t) &= -e^{-\frac{\lambda}{2} u}\, \omega \frac{\sin(\Omega\, u)}{\Omega} \\ a_{T,h}(t) &= -a_{h,T}(t) \\ a_{T,T}(t) &= e^{-\frac{\lambda}{2} u} \left[\cos(\Omega\, u) - \frac{\lambda}{2} \frac{\sin(\Omega\, u)}{\Omega} \right]. \end{aligned} \tag{26}$$

Preprints (www.preprints.org) | NOT PEER-REVIEWED | Posted: 13 September 2018 doi:10.20944/preprints201809.0239.v1

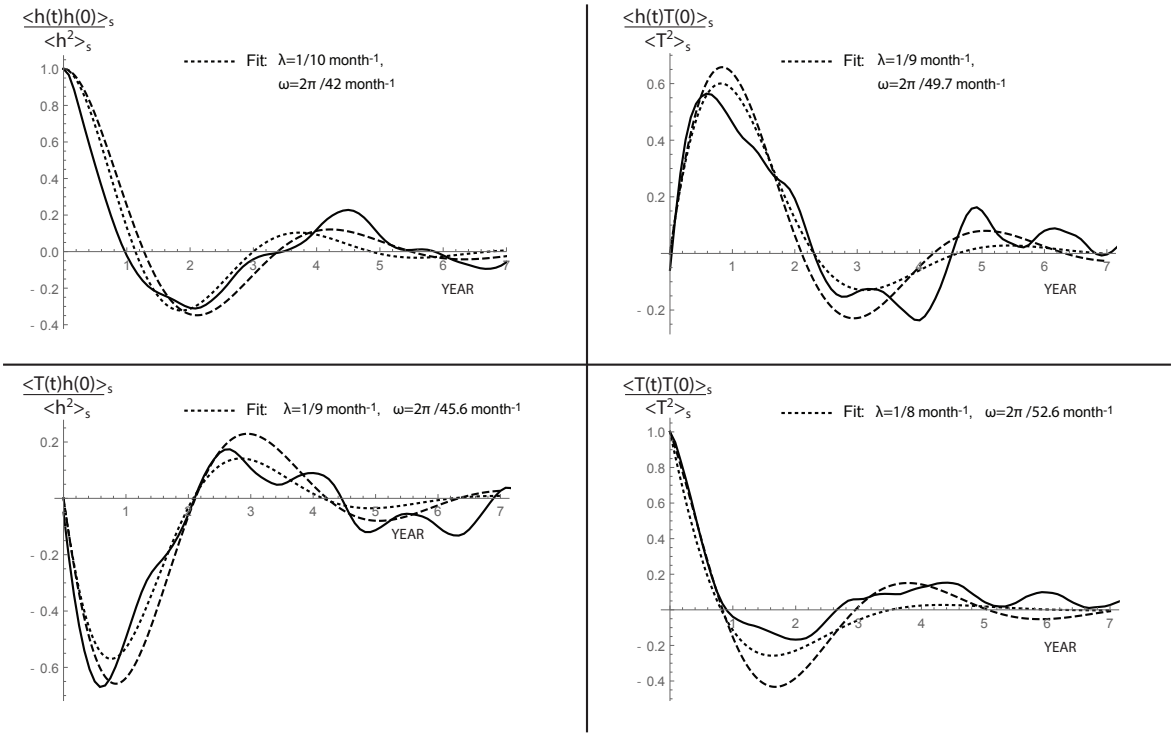

Figure 4. Correlation matrix $\langle x(t)y(0)\rangle_s / \langle y^2\rangle_s$, where "$x$" and "$y$" can be either h or T. Solid line: from the NOAA data (the h values are taken from [42] and refer to the anomalies of the volume of warm water (WWV) in the basin 120E-80W, 5S-5N, in the time range from January 1982 to December 2017). Dashed line, from the FPE of the ROM, i.e. from Eqs. (26)-(27) in the case where $\omega = 2\pi/48\,\text{month}^{-1}$ and $\lambda = 1/12\,\text{month}^{-1}$. Dotted line: a fit with the same functions of Eqs. (26)-(27).

Exploiting Eq. (25), Eq. (24) becomes:

$$\begin{aligned}\langle h(t)h(0)\rangle_s &= \langle h^2\rangle_s\, a_{h,h}(t)\\ \langle T(t)h(0)\rangle_s &= \langle h^2\rangle_s\, a_{T,h}(t)\\ \langle h(t)T(0)\rangle_s &= \langle T^2\rangle_s\, a_{h,T}(t)\\ \langle T(t)T(0)\rangle_s &= \langle T^2\rangle_s\, a_{T,T}(t)\end{aligned} \quad , \tag{27}$$

where (see Eq. (23)) $\langle T^2\rangle_s = \langle h^2\rangle_s \sim D/\lambda \sim 0.63 \pm 0.3$. In Fig. (4) we show the time evolution of the elements of the correlation matrix obtained from observations and the best fit obtained with Eq. (26). This best fit yields values of $\omega = 2\pi/48\,\text{month}^{-1}$ and $\lambda = 1/10\,\text{month}^{-1}$, but the residuals of these fitting functions are quite large. For that, in the same figure we also insert the plot of the same functions of Eq. (26), but with the ROM coefficients given by $\omega = 2\pi/48\,\text{month}^{-1}$ and $\lambda = 1/12\,\text{month}^{-1}$ that, as we shall see later, well agree also with other aspects of the data analysis.

After the above results, it is not surprising that also the power spectrum analysis of the NINO3 data shown in Fig. 5 does not allow us to infer the non Gaussian character of the ENSO statistics. In fact, although in Fig. 5 the power spectrum is evaluated directly as the periodgram of the observed NINO3 index, it is well known that it is directly related to the Fourier transform of the autocorrelation function of T, which, in our ROM with CAM forcing, does not depend on β (see Eqs. (26)-(27)). From a quantitative point of view the comparison of the observed and theoretical spectra in Fig. 5 confirms the already found values for the unperturbed ROM parameters: $\omega = 2\pi/48\,\text{month}^{-1}$, $\lambda = 1/10\,\text{month}^{-1}$.

Preprints (www.preprints.org) | NOT PEER-REVIEWED | Posted: 13 September 2018 doi:10.20944/preprints201809.0239.v1

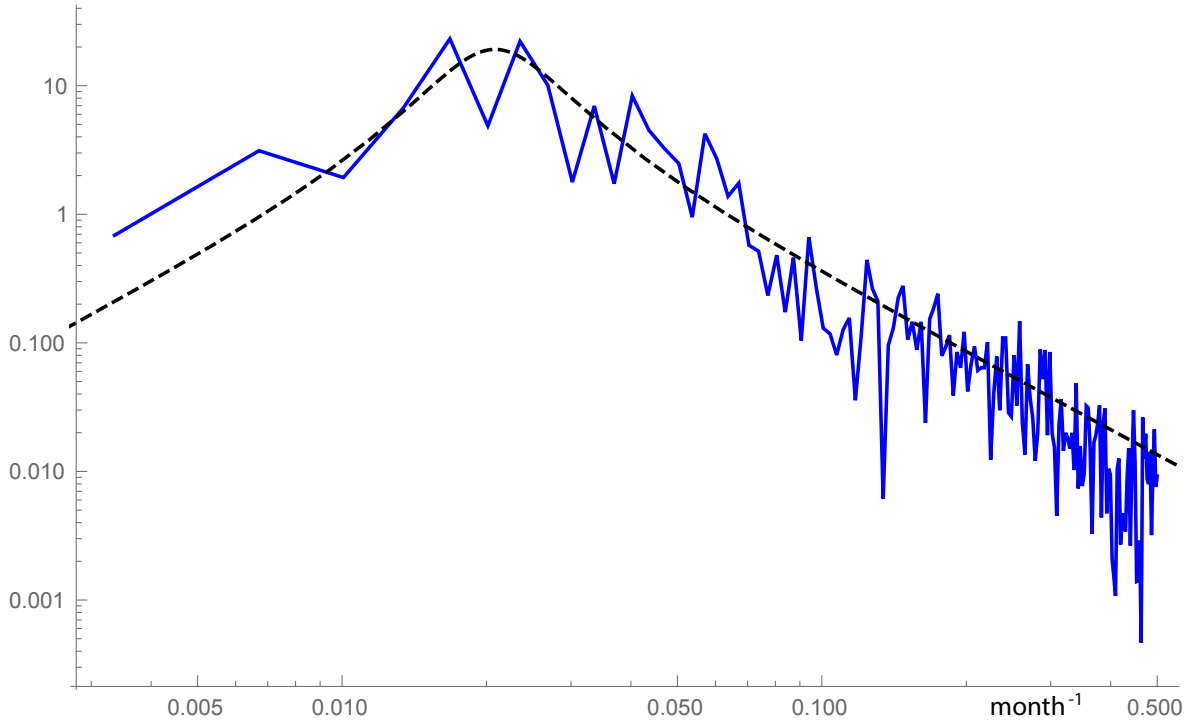

Figure 5. Solid blue line: periodgram of the NINO3 data from NOAA evaluated averaging over non overlapping partitions of length 300 months. Dashed black line: theoretical power spectrum of a ROM with $\omega = 2\pi/48\,\text{month}^{-1}$, $\lambda = 1/10\,\text{month}^{-1}$ and *additive* white noise perturbation.

5.3. Where the nonlinear perturbation plays the main role: the skewed stationary PDF and the recurrence time of strong events

As we have already noticed, if we focused on the first and second moments of the ENSO we would not be able to estimate the value of the parameter β responsible for the nonlinearity of the perturbed ROM of Eq. (15) (or the FPE of Eq. (17)). To infer the value of the β parameter we have to focus our attention on the non Gaussian character of the ENSO statistics, hence we have to evaluate the stationary PDF of the FPE of Eq. (17). Although this FPE is simplified with respect to the more general one (Eq. (18)), the exact stationary PDF is not known. It has been shown in [8], using a reasonable ansatz, that it is possible to obtain the following analytic expression for the reduced stationary PDF of the sole T variable (see also Appendix C):

$$\begin{aligned} p_s(T) &= \beta f_\mu\left(\frac{\mu-2}{1+\beta T}\right) \quad \text{for } T > -1/\beta \\ p_s(T) &= 0 \quad \text{for } T \le -1/\beta, \end{aligned} \tag{28}$$

$$\mu \equiv 1 + \frac{\lambda}{D\beta^2}, \tag{29}$$

where the Gamma-like density function $f_\mu(x)$ is defined as

$$f_\mu(x) \equiv \frac{1}{(\mu-2)\Gamma(\mu-1)} e^{-x} x^\mu, \tag{30}$$

in which $\Gamma(a)$ is the standard complete Gamma function. This stationary PDF depends only on the value of the β parameter that controls the relative intensity of the multiplicative part of the perturbation,

Preprints (www.preprints.org) | NOT PEER-REVIEWED | Posted: 13 September 2018 doi:10.20944/preprints201809.0239.v1

and on the ratio D/λ via the μ parameter of Eq. (29). Notice that, as shown in Eq. (23), D/λ is the stationary variance of T. It is easy to check analytically that in the limit $\beta \to 0$ and D/λ fixed, the stationary PDF in Eqs. (28)-(30) becomes a standard Gaussian, with the same variance D/λ. However, for $\beta \neq 0$ the stationary PDF is clearly non Gaussian. In fact for large positive T it has a "power law" tail that makes it possible to have large fluctuations of positive values of T (strong El Niño events). From Eq. (29) we have that the μ parameter, which controls the behavior of this "heavy" tail of the stationary PDF, strongly depends on the value of the β parameter. The maximum of the stationary PDF is found at $T_{max} = -2/(\beta\mu) \approx -2\beta\, D/\lambda$; for fixed D/λ it is proportional to β. The probability of strong negative values of T (La Niña events) is largely reduced and it is null for temperatures smaller thant the threshold $T_{min} = -1/\beta$.

This skewed stationary PDF for T fits well the data from observations (see (Fig. 1)) with $\beta = 0.2$ and $D/\lambda = 0.62$ ($\mu = 41.42$). The value for D/λ is in agreement with the range of values we have already obtained for the variance of the ROM, hence from now on we set $D/\lambda = 0.62$ and $\beta = 0.2$.

From the FPE of Eq. (17) and using the same ansatz that leads to the stationary PDF in Eqs. (28)-(30), it is also possible to obtain an analytical expression for the mean First Passage Time (FPT) for the ENSO events [44] and to compare these results with the observations. More precisely, we are interested in the average time we have to wait for the onset of a "strong" El Niño event, starting from a "neutral" initial condition defined as the case when the temperature T_i has a value in the range $-0.5 \leq T_i \leq 0.5$. As depicted in Fig. 6, "strong" El Niño events are identified by the criterion $T > 1.5$. Thus, the FPT is defined as the time $\delta t(T_i|T_{tg})$ when $T(t)$ first crosses a given target T_{tg}, starting from the initial value T_i (see Fig. 7). But if $T(t)$ is a stochastic process, repeating many times the same "experiment" should lead to different values for $\delta t(T_i|T_{tg})$, so that the FPT itself is a stochastic process, with its own PDF. We indicate with $t_n(T_i|T_{tg})$ the n^{th} moment of the PDF of the FPT. Of course, the mean FPT is given by $t_1(T_i|T_{tg})$. As we have shown in [44], we have

$$t_1(T_i|T_{tg}) = \left\{ \frac{2}{p_s(T)} \frac{\beta}{2\lambda} \frac{M\left[1, -(\mu-2), -\frac{\mu-2}{\beta T+1}\right]}{\beta T+1} \right\}_{T_i}^{T_{tg}}, \tag{31}$$

where $\{g(x)\}_a^b \equiv g(b) - g(a)$, and $M[1, \alpha, y]$ is the Kummers (generalized hypergeometric) function of the first kind with first argument equal to one. We plot Eq. (31 in Fig. 8 to show the dependence of the mean FPT on T_{tg} for different values of the λ parameter.

From this figure we see that $\lambda = 1/12$ months^{-1}, i.e., a value at the lower end of the expected λ range, provides the best agreement between observational estimates and our analytic result for the mean FPT. With $\lambda = 1/12$ months^{-1}, the mean FPT for intermediate target temperatures, obtained from Eq. (31), is in the range 2-7 years, in good agreement with the observed intervals between intermediate El Niño events. Apart from the inverse proportionality relationship with the relaxation coefficient λ, it is also clear that the average FPT has a strong sensitivity to the value of the β parameter (once the variance $\sigma^2 \sim D/\lambda$ is kept fixed, the μ parameter depends only on β as $\sim 1/\beta^2$). In Fig. 9 we compare the average FPT of Eq. (31) with the values obtained through the numerical integration of the stochastic differential equation equivalent to the FPE of Eq. (17) using $\beta = 0.2$. We can see that there is a good agreement between the analytical and numerical solutions. In the same figure we also show the analytical solutions of the average FPT in the case of a pure additive perturbation ($\beta = 0$, in which case the reduced stationary PDF for the T variable is Gaussian) and for $\beta = 0.3$. For weak to intermediate El Niño events ($T_{tg} \leq 1.5$), the average FPT depends weakly on β. However, the sensitivity to β clearly emerges in the case of strong and very strong events. In particular, the purely additive forcing leads to average FPT that are many order of magnitude larger than those obtained with $\beta = 0.2$ (note the logarithmic scale in the ordinate of the graph), while in the case of $\beta = 0.3$ the FPTs are shorter at large T_{tg}.

Preprints (www.preprints.org) | NOT PEER-REVIEWED | Posted: 13 September 2018 doi:10.20944/preprints201809.0239.v1

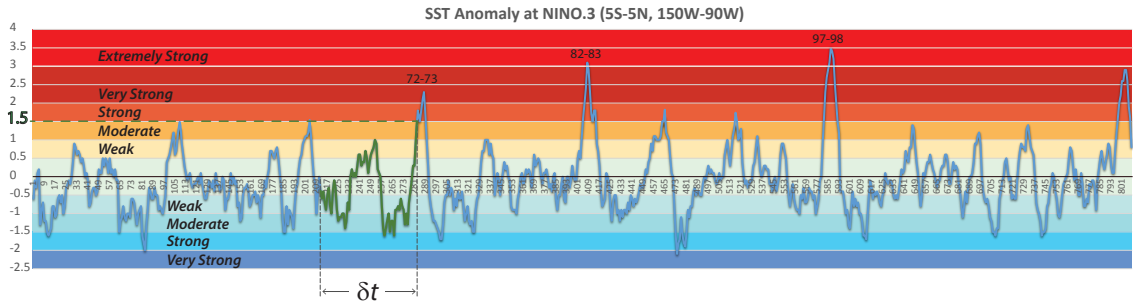

Figure 6. The month averaged NINO3 data from Jan-1949 to Feb-2016. Data are from the Tokyo Climate Center, WMO Regional Climate Centers (RCCs) [43]. In green we highlight a segment of the time series to illustrate the First Passage Time (FPT) $\delta t(T_i, T_{tg})$ for a given target temperature anomaly T_{tg} (here $T_{tg} = 1.5$), starting from an initial neutral temperature T_i ($-0.5 \leq T_i \leq 0.5$). See also the text and Fig. (7) for details about the FPT.

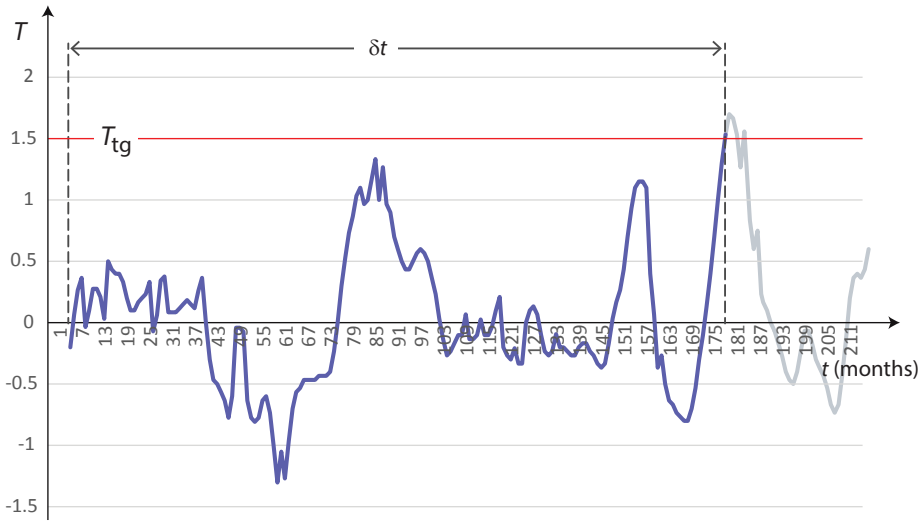

Figure 7. The First Passage Time $\delta t(T_i, T_{tg})$ for a target temperature anomaly of $T_{tg} = 1.5$ is defined as the first time the fluctuating temperature $T(t)$ cross the threshold T_{tg} (1.5 in this case), starting from an initial temperature T_i (that we will choose in the range $-0.5 \leq T_i \leq 0.5$, corresponding to neutral ENSO conditions).

5.4. Inferring the FPE coefficients from data

The results of the previous sections validate the FPE of Eq. (17) with parameters $\omega = 2\pi/48\,\text{month}^{-1}$, $\lambda = 1/12\,\text{month}^{-1}$ and $D/\lambda = 0.62$. However, at least in principle, there is a way to infer the transport coefficients of a FPE directly from data. For that purpose, let us rewrite the FPE of Eq. (17) in the following way:

$$\partial_t \sigma(h, T; t) = \left\{ -\partial_h G_h(h, T) - \partial_T G_T(h, t) + \partial_T^2 A(T) \right\} \sigma(h, T; t), \tag{32}$$

where (as in Eq. (22) we used the transformation $h \to h + \beta D/\omega$ to eliminate the mean value of the thermocline depth anomaly)

$$\begin{aligned} A(T) \equiv & D(1 + \beta\, T)^2 \\ G_T(h, T) \equiv & \omega\, h - (\lambda - D\,\beta^2)\, T \\ G_h(h, T) \equiv & -\omega\, T. \end{aligned} \tag{33}$$

Preprints (www.preprints.org) | NOT PEER-REVIEWED | Posted: 13 September 2018 doi:10.20944/preprints201809.0239.v1

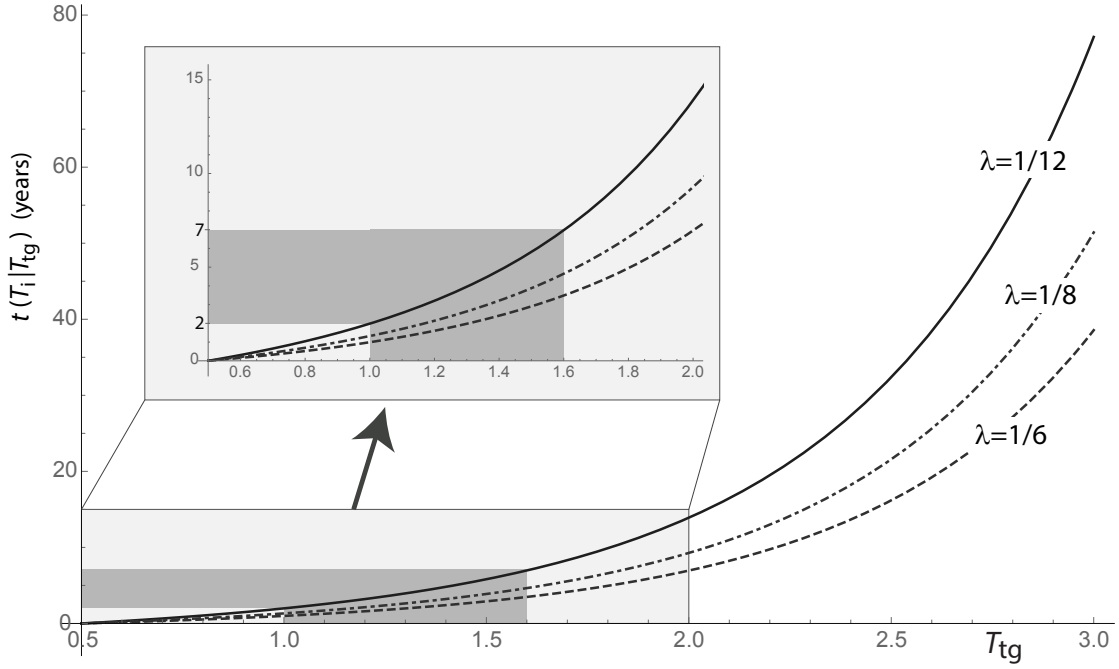

Figure 8. The mean FPT for different values of the λ parameter, vs the target temperature, obtained using Eq. (31). The values of β and μ have been fixed by fitting the stationary PDF of Eqs. (28)-(30) to NINO3 from [39]: $\beta = 0.2$ and $\mu = 41.42$ (see text for details). Dashed line: $\lambda = 1/6\,\text{month}^{-1}$, dot-dashed line $\lambda = 1/8\,\text{month}^{-1}$, solid line $\lambda = 1/12\,\text{month}^{-1}$. In the inset, a zoom of the same graphs, where the gray background emphasizes the range 2-7 years and $1.0 \leq T \leq 1.6$, corresponding to the typical recurring times interval for intermediate El Niño events. Notice how the curve obtained with $\lambda = 1/12\,\text{month}^{-1}$ falls better than the others in this zone.

It is well known that given the FPE of Eq. (17), the drift and diffusion coefficients can be inferred using their statistical definitions as conditional first and second moments of the process increments [46–48]:

$$A(T) = \frac{1}{2}\lim_{\delta t\to 0}\frac{1}{\delta t}\int_{-\infty}^{\infty}(T-T')^2 P(h',T'|h,T;\delta t)\,\mathrm{d}h'\mathrm{d}T' \tag{34a}$$

$$G_T(h,T) = \lim_{\delta t\to 0}\frac{1}{\delta t}\int_{-\infty}^{\infty}(T-T') P(h',T'|h,T;\delta t)\,\mathrm{d}h'\mathrm{d}T' \tag{34b}$$

$$G_h(h,T) = \lim_{\delta t\to 0}\frac{1}{\delta t}\int_{-\infty}^{\infty}(h-h') P(h',T'|h,T;\delta t)\,\mathrm{d}h'\mathrm{d}T', \tag{34c}$$

in which $P(h',T'|h,T;\delta t)$ is the conditional probability to go from (h,T) to (h',T') in an infinitesimal time δt. From a practical viewpoint, the above expressions are obtained from the expectation values of the first (Eqs. (34b)- (34c)) and second (Eq. (34a)) moments of the difference of two subsequent NINO3 values, where the time step is $\delta t = 1$ month. Because the duration of the h time series is too short to obtain a reliable two dimensional PDF (note that for h we use the "proxy" given by the anomalies in the volume of warm water (WWV) in the basin 120E-80W, 5S-5N, in the time range from January 1982 to December 2017, taken from [42]), we focus our attention only on the T variable, i.e., we work only with the observed Niño3 index. This means that we disregard the drift coefficient of Eq. (34c), and, for each T value, when we evaluate the expectation of the first and second moments of the process increments of T, we automatically average over h at fixed T. This average over the h variable does not affect the diffusion coefficient of Eq. (34a), thus,

$$\frac{\mathbb{E}[(T(t+\delta t)-T(t))^2]}{2\,\delta t} = A(T) = D(1+\beta\,T)^2, \tag{35}$$

Preprints (www.preprints.org) | NOT PEER-REVIEWED | Posted: 13 September 2018 doi:10.20944/preprints201809.0239.v1

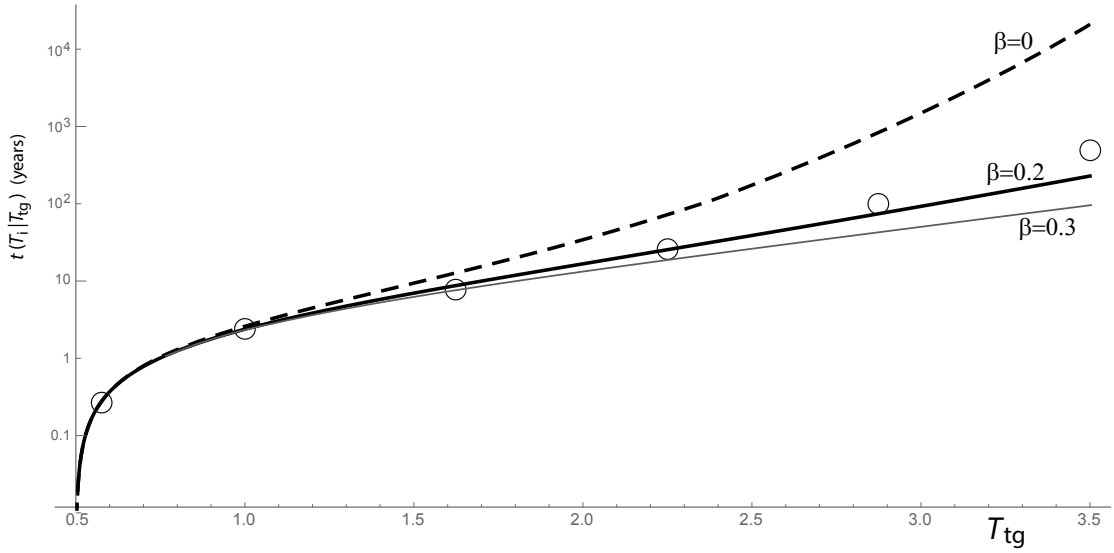

Figure 9. Semi-log plot of the average FPT as a function of the target temperature T_{tg}, for $\lambda = 1/12\,\text{month}^{-1}$ and $\sigma^2 = D/\lambda = 0.62$ (see text for details). Thick solid line: Eq. (31) with $\beta = 0.2$. Thin solid line: Eq. (31) with $\beta = 0.3$. Thick dashed line: Eq. (31) with $\beta = 0$, corresponding to the pure additive forcing of the ROM. Circles, FPT from numerical simulation of the Îto SDE [45] corresponding to the FPE of Eq. (17): $\dot{h} = -\omega T$; $\dot{T} = -\omega h + D\beta - (\lambda - D\beta^2)T + \sqrt{D}(1+\beta T)\xi$, where ξ is a white noise with correlation $\langle \xi(t)\xi(0)\rangle = \delta(t)/2$, $\beta = 0.2$, and $\omega = 2\pi/48\,\text{month}^{-1}$.

while for the drift coefficient of Eq. (34b) we have:

$$\frac{\mathbb{E}[T(t+\delta t) - T(t)]}{\delta t} = \langle G_T(h,T)\rangle_{T,s} \equiv -\left(\lambda - D\,\beta^2\right) T \simeq -\lambda\, T, \tag{36}$$

where $\langle ...\rangle_{T,s}$ means the conditional stationary average at fixed T.

The functions in Eqs. (35) and (36)) correspond to the diffusion and drift coefficients, respectively, of the following reduced FPE for the T variable:

$$\partial_t\, p(T;t) = \left\{ (\lambda - D\,\beta^2)\partial_T T + \partial_T^2 D(1+\beta T)^2 \right\} p(T;t), \tag{37}$$

that is, the same FPE we would obtain directly by using the already cited ansatz introduced in [8], in the FPE of Eqs. (17)-(33). In Figure 10 we see that from the NINO3 data the expectation value $\mathbb{E}[T(t+\delta t) - T(t)]$ looks as a linear function of T, *supporting again the view of a linear unperturbed ROM*, and the linear fit is very close to $-\lambda\, T$ with $\lambda = 1/12\,\text{month}^{-1}$, the same values we have obtained from the mean FPT analysis of the previous sub-Section.

Concerning the diffusion coefficient, evaluated as in Eq. (34a), we see from Fig. (11) that the expectation value $\mathbb{E}[(T(t+\delta t) - T(t))^2]/2$ is compatible with the square dependence on T of Eq. (35), but the the uncertainty is large. This large uncertainty is due to the nonlinear nature of $A(T)$, which makes the fitting process strongly dependent on large T values where the statistics is poor.

6. Discussion and conclusions

Starting from the fact that the ENSO statistics has some clear non Gaussian features, in this paper we discuss which non-linear dynamics might be responsible for them. We consider the ENSO as the result of the interaction between some slow oceanic variables (the unperturbed Recharge Oscillator Model-ROM) and a fast fluctuating forcing (modeling both atmosphere and ocean components) and we obtain the corresponding Fokker Plank Equation (FPE). In this simplified model, we consider

Preprints (www.preprints.org) | NOT PEER-REVIEWED | Posted: 13 September 2018 doi:10.20944/preprints201809.0239.v1

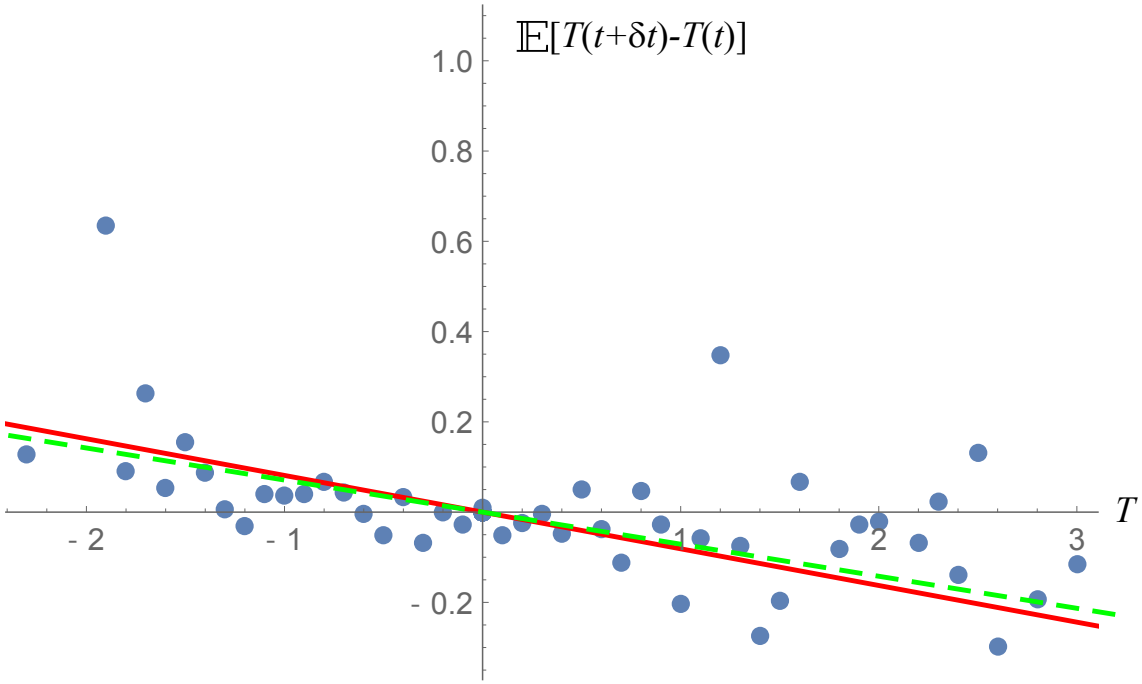

Figure 10. Dots: the expectation value $\mathbb{E}[T(t+\delta t) - T(t)]$ where $\delta t = 1$ month, of the NINO3 data from http://www.cpc.ncep.noaa.gov/data/indices compared with the drift coefficient $\langle G_T(h,T)\rangle_{T,s} \simeq -\lambda T$ (see Eq. (36)), in the cases where the coefficient λ is obtained as the the best fit to the data (dashed green line), from which $\lambda = 1/13.7\,\text{month}^{-1}$, and the case where $\lambda = 1/12\,\text{month}^{-1}$ (solid red line, see text for details). For large absolute values of T the spreading of the data around the linear fit increases because the number of registered ENSO events decreases (e.g., just one for $T = -2$).

Preprints (www.preprints.org) | NOT PEER-REVIEWED | Posted: 13 September 2018 doi:10.20944/preprints201809.0239.v1

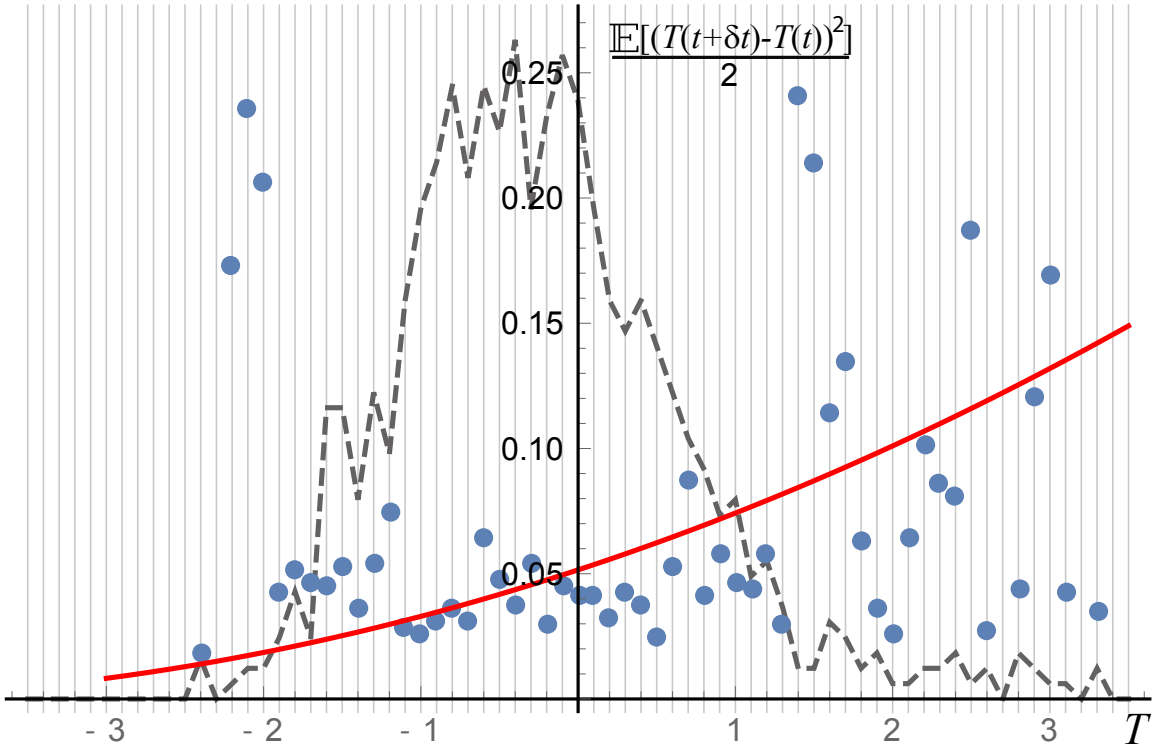

Figure 11. Dots: the expectation value $\mathbb{E}[(T(t+\delta t)-T(t))^2]/2$ where $\delta t = 1$ month, of the Niño3 data from http://www.cpc.ncep.noaa.gov/data/indices. Solid red line:the diffusion coefficient $\langle A(T)(h,T)\rangle_{T,s} = D(1+\beta T)^2$ (see Eq. (35)), where $\beta = 0.2$ and $D = \sigma^2\lambda = 0.62\,\text{month}^{-1}$ (see text for details). Gray dashed line: number of observed events for each point of the plot, scaled by a factor $1/160$ in the vertical axes. The points for extreme events are not that close to the theoretical red line, but in these cases the statistics is also really poor.

Preprints (www.preprints.org) | NOT PEER-REVIEWED | Posted: 13 September 2018 doi:10.20944/preprints201809.0239.v1

two possible sources of nonlinearity: nonlinearity in the dynamics of the unperturbed ROM, and a non linear (i.e., multiplicative) fast perturbation of the ROM. Comparison with observations leads to the conclusion that the observed non Gaussianity is due to the non linear fast perturbation of the ROM, while the (possible) non linearity in the dynamics of the ROM plays (if any) a minor role. We further use our approach to determine the First Passage Time (FPT) of ENSO events. By fitting our theoretical results to the data we are able to estimate the ROM/FPE key parameters, namely ω, λ, D and β: $\omega = 2\pi/48\,\text{month}^{-1}$, $\lambda = 1/12\,\text{month}^{-1}$, $D = 0.62\,\lambda$ and $\beta = 0.2$.

Observation data are also used to infer directly the FPE coefficients. We are able to validate once more the assumption of a linear internal dynamics of the ROM (Fig. 10) and of a non-constant diffusion (Fig. 11) coefficient. At a quantitative level, however, the exact relationship between T and the diffusion coefficient is difficult to determine with accuracy because nonlinearities become important in the large T range (rare events), where the statistics is rather poor (dashed line in Fig. 11).

We can conclude that the nonlinear interaction between the fast and slow modes of the ENSO gives the substantial contribution to the non Gaussianity of the ENSO statistics. However, further work is necessary to better quantify the nonlinear nature of the perturbation, which is related to the nonlinear diffusion coefficient of the FPE. For example one could add a constant diffusion term D_1 (due to another additive forcing $\zeta(t)$ of the ROM, uncorrelated with $\xi(t)$) to the quadratic term $A(T)$ of Eq. (35) . It turns out that the sum $D_1 + A(T)$ fits to the data in Fig. 11 as well as $A(T)$ alone, but with an increased value for β and a decreased value for D. Thus, to be able to define the actual D_1 and β values we should increases the sample size used for the fitting process, for example using longer time series from century long reanalysis products (CERA 20C, https://www.ecmwf.int/en/forecasts/datasets/archive-datasets/reanalysis-datasets/cera-20c).

Conflicts of Interest: The authors declares no conflict of interest.

Appendix A Validation of the linear relationship between the wind stress and T_E

Eq. (4) is an assumption that agrees with observations as shown in the following. The wind stress is considered proportional to the square of the wind velocity at 10m from sea surface taken from [25]. Figure A1 shows the equatorial zonal (i.e., averaged over 5S-5N) wind velocity for different longitudes. We see that very close to the America's coast (81W) the direction of the wind flips from trade wind to Westerly. This is due to the thermal gradient we have when we pass from the cold East Pacific equatorial ocean to the warm central America lands. Thus for the wind stress τ_s of Eq. (4) we use the anomaly (i.e., 1948-2018 mean removed) of the equatorial zonal wind stress averaged in the longitude interval 180W-120W. The fluctuating quantity τ_s is divided in a slow ($\tau_{s,slow}$) and fast ($\tau_{s,fast}$) components. The $\tau_{s,slow}$ data are obtained from the one year average of τ_s data, while $\tau_{s,fast} \equiv \tau_s - \tau_{s,slow}$. Then:

1) from Figure A2 we clearly see that the time behavior of $\tau_{s,slow}$ and $T_{E,slow}$ are similar (of course, some lag remains between the wind stress, that is a a forcing term, and the ocean reaction);
2) From Figures A3 we see that the plot of the cross correlation between $\tau_{s,slow}$ and $T_{E,slow}$ vs time (in moths) is very similar to the plot of the autocorrelation of $T_{E,slow}$ (notice the little time offset between these two plots, indicating the fact that the one year time average has not completely hidden the cause-effect relationship between $\tau_{s,slow}$ and $T_{E,slow}$). Moreover, from the insert of the same Figure we see that the average relationship between $\tau_{s,slow}$ and $T_{E,slow}$ is mainly linear, with a small dispersion of the data around the linear fit (quantities are normalized by the standard deviation of the quantities from observations):

$$\tau_s \equiv \tau_{s,slow} + \tau_{s,fast} = k\,T_E + \tau_{s,fast}. \tag{A1}$$

The above two arguments strongly support the hypothesis expressed by Eq. (4).

Preprints (www.preprints.org) | NOT PEER-REVIEWED | Posted: 13 September 2018 doi:10.20944/preprints201809.0239.v1

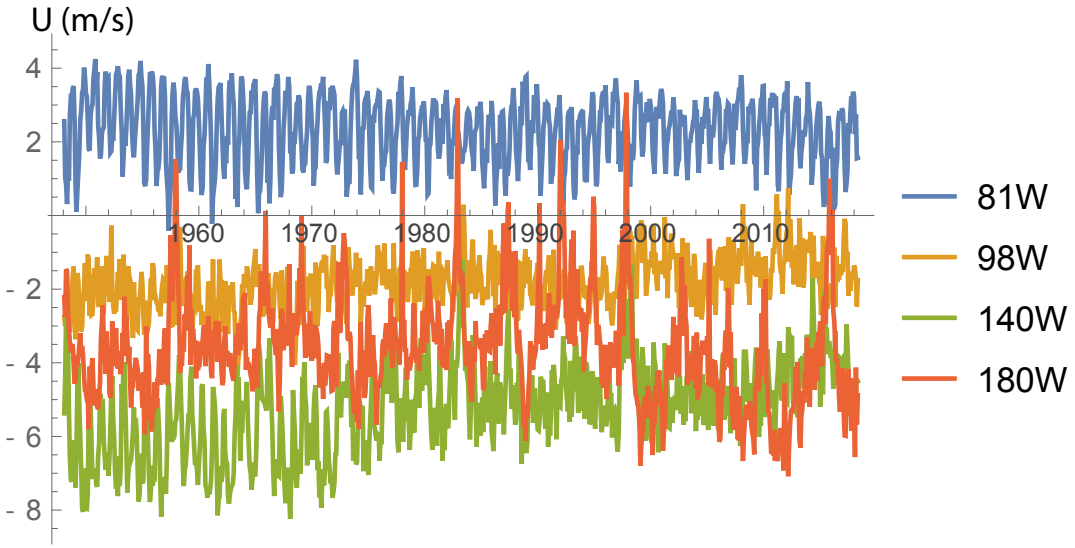

Figure A1. 5N-5S averaged zonal wind for different longitudes. Data from NOAA [25]

Appendix B Very short review of the projection approach applied to the ROM

In the present work we study the same ROM considered in [8], however we do not use the FPE in Eqs. (3)-(4) of [8] because of a marginal mistake: a missing additive term in the FPE, that here we want to fix. Thus, for the reader convenience, in the following we give a short summary of the projection procedure adapted to the present case.

The idea of this approach is to assume that the fast fluctuating force $\xi(t)$ has a deterministic nature, namely that the ROM of Eq. (15) is just a part of a set of equations describing a larger deterministic system:

$$\begin{aligned} \dot{h} &= -\omega\, T \\ \dot{T} &= \omega\, h - \lambda T + \epsilon\, \xi(1+\beta T) \\ \dot{\xi} &= F\left(\xi, \boldsymbol{\pi}\right) \\ \dot{\boldsymbol{\pi}} &= \boldsymbol{Q}\left(\xi, \boldsymbol{\pi}\right). \end{aligned} \tag{B1}$$

Using the terminology of the projection approach [31,38,49] the ROM is viewed as the "system of interest" (or system a), while $(\xi, \boldsymbol{\pi})$ represent the *booster* system (or "rest of the system" or system b), namely a set of general chaotic and fast variables, e.g., the MJO and WWB [50–54], that, perturbing the ROM activate the El Niño/La Niña phenomena and which obey some *unspecified* equations of motion expressed by the *generic* functions $F\left(\xi, \boldsymbol{\pi}\right)$ and $\boldsymbol{Q}\left(\xi, \boldsymbol{\pi}\right)$. The value of the parameter ϵ determines the intensity of the perturbation to the ROM. For $\epsilon = 0$ the first two lines of Eq. (B1) define the unperturbed system of interest (or unperturbed ROM).

We stress that we leave unspecified the exact expressions of the functions $F\left(\xi, \boldsymbol{\pi}\right)$ and $\boldsymbol{Q}\left(\xi, \boldsymbol{\pi}\right)$, representing the equation of motion for the booster, because we do not need to know them in details (the booster typically will be a *non linear* chaotic system); it is enough that they satisfy some specific assumptions as detailed in the following.

More generally, the interaction between the ROM and the booster should be bi-directional: the booster equation of motion should be affected by the dynamics of the ROM: $F = F\left(\xi, \boldsymbol{\pi}, \epsilon\, R(h,T)\right)$ and $\boldsymbol{Q} = \boldsymbol{Q}\left(\xi, \boldsymbol{\pi}, \epsilon\, R(h,T)\right)$. The function $\epsilon\, R(h,T)$ is the "reaction" force of the ROM variables on the MJO/WWB system. However, for the sake of simplicity we shall consider hereafter $\epsilon\, R(h,T) = 0$ as in [8]. The feedback term can be included following the general approach of [55,56]. The goal is to

Preprints (www.preprints.org) | NOT PEER-REVIEWED | Posted: 13 September 2018 doi:10.20944/preprints201809.0239.v1

describe the statistics of the part of interest. We start from the following Langevin equation for the PDF $\rho(h, T, \xi, \boldsymbol{\pi}; t)$ of the total system:

$$\partial_t \rho(h, T, \xi, \boldsymbol{\pi}; t) = \{\mathcal{L}_a + \epsilon\, \mathcal{L}_I \xi + \mathcal{L}_b\}\, \rho(h, T, \xi, \boldsymbol{\pi}; t) \tag{B2}$$

where the unperturbed and perturbation Liouville operators, are given by

$$\begin{aligned} \mathcal{L}_a &= \omega\, \partial_h T - \omega\, \partial_T h + \lambda\, \partial_T T \\ \mathcal{L}_I &= -\partial_T (1 + \beta\, T), \end{aligned} \tag{B3}$$

respectively. In Eq. (B2) we do not write the explicit expression of the Liouville operator $\mathcal{L}_b$ of the booster because it is related to the unknown functions $F(\xi, \boldsymbol{\pi})$ and $\boldsymbol{Q}(\xi, \boldsymbol{\pi})$.

We are interested in obtaining a Fokker Plank Equation (FPE) for the reduced (or marginal) PDF of the system of interest, given by $\sigma(h, T; t) \equiv \int \rho(h, T, \xi, \boldsymbol{\pi}; t) \mathrm{d}\xi \mathbf{d}\boldsymbol{\pi}$. Introducing the projection operator, $\mathbb{P} \cdots \equiv \wp_b(\xi, \boldsymbol{\pi}) \int \mathrm{d}\xi \mathbf{d}\boldsymbol{\pi} \cdots$, where $\wp_b$ is the stationary PDF of the booster, defined by $\wp_b(\xi, \boldsymbol{\pi}) \mid \mathcal{L}_b \wp_b(\xi, \boldsymbol{\pi}) = 0$, we have: $\sigma(h, T; t) = 1/\wp_b(\xi, \boldsymbol{\pi}) \times \mathbb{P}\rho(h, T, \xi, \boldsymbol{\pi}; t)$. Following the Zwanzig-like formal projection approach in the perturbation version of [29–31] to the lowest non vanishing order on the coupling parameter ϵ, the time evolution of $\sigma(h, T; t)$ is governed by the following integro-differential equation:

$$\begin{aligned} &\partial_t \sigma(h, T; t) = \mathcal{L}_a\, \sigma(\boldsymbol{x}; t) \\ &+ \epsilon^2 \langle \xi^2 \rangle_b \left\{ \mathcal{L}_I \int_0^\infty \mathrm{d}u\, \varphi(u)\, e^{\mathcal{L}_a u} \mathcal{L}_I e^{-\mathcal{L}_a u} \right\} \sigma(h, T; t) \end{aligned} \tag{B4}$$

In the above equation $\varphi(u)$ is the normalized auto-correlation function of the booster variable ξ and $\langle \xi^2 \rangle_b$ is the variance of ξ (without any loss of generality, we assumed $\langle \xi \rangle_b = 0$). A very important outcome of Eq. (B4) is that *we can group all the possible booster dynamical systems in different classes of equivalence, where all the boosters belonging to the same class give rise to the same statistical properties for a given system of interest*. In fact, the FPE depends only on the booster autocorrelation function $\langle \xi^2 \rangle_b \varphi(u)$: different dynamical systems that share the same autocorrelation function, belong to the same booster class of equivalence. Given Eq. (B3), we can rewrite Eq. (B4) as:

$$\begin{aligned} \partial_t \sigma(h, T; t) = \Big\{ &\partial_h \omega\, T - \partial_T \omega\, h + \lambda\, \partial_T T \\ &+ \beta\, \epsilon^2 \langle \xi^2 \rangle_b\, \tau\, \partial_T (1 + \beta\, T) \\ &+ \epsilon^2 \langle \xi^2 \rangle_b\, \partial_T (1 + \beta\, T) \\ &\times \int_0^\infty \mathrm{d}u\, \varphi(u) \big(1 + \beta\, T_a(h, t; -u)\big) e^{\mathcal{L}_a u} \partial_T e^{-\mathcal{L}_a u} \Big\} \sigma(h, T; t), \end{aligned} \tag{B5}$$

where we have used the identity $\partial_T (1 + \beta\, T) = (1 + \beta\, T)\partial_T + \beta$ (this last term was the cited missed one in [8] and it is not vanishing when the interaction with the booster is not Hamiltonian as in the present case) and we have introduced the decay time of the booster autocorrelation function as $\tau \equiv \int_0^\infty \mathrm{d}u \varphi(u)$. Moreover, in the above equation we have exploited the result $\exp[\mathcal{L}_a u] T \exp[-\mathcal{L}_a u] = T_a(h, t; -u)$ (see for example Eqs. (31)-(32) of [38]), where $T_a(h, t; -u)$ and $h_a(h, t; -u)$ (for further use) are the unperturbed ($\epsilon = 0$) back time evolution for a time u of the T and the h variables, respectively, starting from the initial condition ($u = 0$) given by $T_a(h, t; 0) = T$ and $h_a(h, t; 0) = h$.

In the case where there is an extremely large time scale separation between the dynamics of the unperturbed ROM and the forcing atmosphere, the autocorrelation function $\varphi(u)$ decays so fast, respect to the typical time scale of the unperturbed ROM, that we can make the following approximations: $T_a(h, t; -u) \sim T$ and $e^{\mathcal{L}_a u} \partial_T e^{-\mathcal{L}_a u} \sim \partial_T$. Thus in this case from Eq. (B5) we obtain the standard result of the theory of stochastic Markovian processes [40], namely the FPE of Eq. (17).

Preprints (www.preprints.org) | NOT PEER-REVIEWED | Posted: 13 September 2018 doi:10.20944/preprints201809.0239.v1

More in general, Eq. (B5) gives the transport coefficients $A(h,T)$ and $B(h,T)$ of Eq. (18) also for the cases where we do not assume such stringent assumptions about the time scale separation between the unperturbed ROM and the fast atmosphere. These have been already given in [8] Supporting Information, by making a link with some final results of [38]. We mention only the fact that the most troublesome problem in order to get $A(h,T)$ and $B(h,T)$ from Eq. (B5) is to manipulate the compound of operators $\exp[\mathcal{L}_a u]\partial_T \exp[-\mathcal{L}_a u]$. For that we refer the reader to the results of [55] and (for a more general approach to the Lie evolution of differential operators) to the more recent work of Ref. [57]. Here we report the final result, that is given by Eq. (19), where ($D \equiv \epsilon^2 \langle \xi^2 \rangle_b \tau$)

$$\begin{aligned} A_0 &= \frac{D}{\tau} \int_0^\infty du\, \varphi(u) e^{-\frac{\lambda}{2}u} \left[\cos(\Omega u) - \frac{\lambda}{2\Omega}\sin(\Omega u)\right] \\ &= \frac{D}{\tau}\left\{\Re\left[\hat{\varphi}(\Omega - \mathrm{i}\lambda/2)\right] + \frac{\lambda}{2\Omega}\Im\left[\hat{\varphi}(\Omega - \mathrm{i}\lambda/2)\right]\right\} \end{aligned} \tag{B6}$$

$$\begin{aligned} A_1 &= -\frac{D}{\tau}\frac{\omega}{2\Omega}\int_0^\infty du\, \varphi(u)\left[\frac{\lambda}{2\Omega}\cos(2\Omega u) + \sin(2\Omega u)\right] \\ &+ \frac{D}{\tau}\frac{\omega\lambda}{4\Omega^2}\int_0^\infty \varphi(u) du \\ &= -\frac{D}{\tau}\frac{\omega}{2\Omega}\left\{\frac{\lambda}{2\Omega}\Re\left[\hat{\varphi}(2\Omega)\right] - \Im\left[\hat{\varphi}(2\Omega)\right]\right\} \\ &+ D\,\frac{\omega\lambda}{4\Omega^2} \end{aligned} \tag{B7}$$

$$\begin{aligned} A_4 &= \frac{D}{\tau}\int_0^\infty du\, \varphi(u)\left[\omega^2(1 + \cos(2\Omega u) - \frac{\lambda^2}{2}\right]\frac{1}{2\Omega^2} \\ &= D\left(1 - \frac{\omega^2}{2\Omega^2}\right) + \frac{D}{\tau}\frac{\omega^2}{2\Omega^2}\Re\left[\hat{\varphi}(2\Omega)\right] \end{aligned} \tag{B8}$$

$$A_2 = A_4 + A_0, \quad A_3 = A_1 \tag{B9}$$

$$\begin{aligned} B_0 &= -\frac{D}{\tau}\frac{\omega}{\Omega}\int_0^\infty du\, \varphi(u) e^{-\frac{\lambda}{2}u}\sin(\Omega u) \\ &= \frac{D}{\tau}\frac{\omega}{\Omega}\Im\left[\hat{\varphi}(\Omega - \mathrm{i}\lambda/2)\right] \end{aligned} \tag{B10}$$

$$\begin{aligned} B_1 &= -\frac{D}{\tau}\frac{\omega^2}{2\Omega^2}\int_0^\infty du\, \varphi(u)\cos(2\Omega u) \\ &+ \frac{D}{\tau}\frac{\omega^2}{2\Omega^2}\int_0^\infty \varphi(u) du \\ &= -\frac{D}{\tau}\frac{\omega^2}{2\Omega^2}\Re\left[\hat{\varphi}(2\Omega)\right] + D\,\frac{\omega^2}{2\Omega^2} \end{aligned} \tag{B11}$$

Preprints (www.preprints.org) | NOT PEER-REVIEWED | Posted: 13 September 2018 doi:10.20944/preprints201809.0239.v1

$$\begin{aligned} B_4 &= -\frac{D}{\tau}\,\frac{\omega}{2\Omega}\int_0^\infty du\,\varphi(u)\left[\sin(2\Omega u)-\frac{\lambda}{\Omega}\cos(2\Omega u)\right] \\ &- \frac{D}{\tau}\,\frac{\lambda}{2}\,\frac{\omega}{\Omega^2}\int_0^\infty \varphi(u)du \\ &= \frac{D}{\tau}\,\frac{\omega}{2\Omega}\left\{\frac{\lambda}{\Omega}\Re\left[\hat{\varphi}(2\Omega)\right]+\Im\left[\hat{\varphi}(2\Omega)\right]\right\} \\ &- D\,\frac{\lambda}{2}\,\frac{\omega}{\Omega^2} \end{aligned} \tag{B12}$$

$$B_2 = B_4 + B_0, \quad B_3 = B_1, \tag{B13}$$

with $\tau = \Re\left[\hat{\varphi}(0)\right]$, the symbols $\Im[\ldots]$ and $\Re[\ldots]$ stand for the imaginary and the real part of $[\ldots]$, respectively and the hat over the function φ means the Fourier transform of this function, having assumed $\varphi(t) = 0$ for $t < 0$: $\hat{\varphi}(\alpha) \equiv \int_0^\infty \exp[-i\alpha u]\varphi(u)du$. The following equalities hold:

$$A_4 + B_3 = D, \quad A_2 + B_1 = A_0 + D. \tag{B14}$$

In the limit of large time scale separation between the ROM and the fast booster we can use the approximations $\Re\left[\hat{\varphi}(x\,\Omega)\right] \sim \Re\left[\hat{\varphi}(0)\right] = \tau$ and $\Im\left[\hat{\varphi}(x\,\Omega)\right] \sim \Im\left[\hat{\varphi}(0)\right] = 0$ in Eqs. (B6)-(B12), and we obtain the standard FPE for an oscillator perturbed by a white noise, given in Eq. (17).

Appendix C The ansatz and the stationary PDF

Here we review Appendix B of Ref. [8], to find the reduced stationary PDF for the T variable. We start from the FPE of Eq. (17), that, after the shift $h \to h + \beta D/\omega$ which annuls the mean value of the anomaly thermocline depth, becomes the FPE of Eqs. (32)-(33). Because we are interested only on the reduced PDF for the T variable, we integrate the h variable in the FPE of Eqs. (32)-(33), to obtain (we remind again that $D \equiv \epsilon^2\langle\xi^2\rangle_b\tau$):

$$\partial_t\, p(T;t) = -\omega\,\partial_T\langle h\rangle_T + \left\{(\lambda - D\beta^2)\partial_T T + \partial_T^2 D(1+\beta T)^2\right\} p(T;t), \tag{C1}$$

where $p(T;t) \equiv \int \sigma(h,T;t)\mathrm{d}h$ is the reduced PDF for the T variable and $\langle h\rangle_T \equiv \int h\sigma(h,T;t)\mathrm{d}h$, is the conditional average value of the h variable (note: $p_s(T) \equiv \int \sigma_s(h,T)\mathrm{d}h$). Because $\omega \sim 0.13$ and $\lambda \sim 0.1$, we are neither in the under-damped, nor in the over-damped standard cases where it is possible to reduce the two-dimensional FPE to the one dimensional type [30,58,59]. However we take advantage of the fact that here we focus our attention on the *stationary* PDF of the reduced FPE, for which $\partial p(T;t)/\partial t = 0$ in Eq. (C1). Thus, observing that the relations among the stationary first and second moments of the h and T variables that we obtain from Eq. (22), are the same of the case of a stochastic damped linear oscillator (see also B_16), we make the following *ansatz*:

$$\langle h\rangle_{T,s} = \langle h\rangle_s\, p_s(T) = 0 \tag{C2}$$

where the former equality represents the *ansatz*.

Inserting Eq. (C2) in the FPE of Eq. (C1), imposing the condition of vanishing current, and using the definition $\mu \equiv 1 + \lambda/(D\,\beta^2)$, we obtain:

$$\beta(2 + \mu\,\beta T)\, p_s(T) + (1+\beta T)^2\partial_T\, p_s(T) = 0. \tag{C3}$$

From the previous equation, we get two results: the stationary PDF has a maximum (i.e. the T derivative vanishes) for $T = -2/(\beta\mu) = -2\beta D/(\lambda + D\,\beta^2)$; the stationary PDF must vanish for $T = -1/\beta$ (and for lesser values too, for obvious physical reasons). As already noted in [8], from Eq. (22), for $(\lambda - 2\beta^2 D) > 0$ (namely, for $\mu > 3$) the equation of motion of the first and second

Preprints (www.preprints.org) | NOT PEER-REVIEWED | Posted: 13 September 2018 doi:10.20944/preprints201809.0239.v1

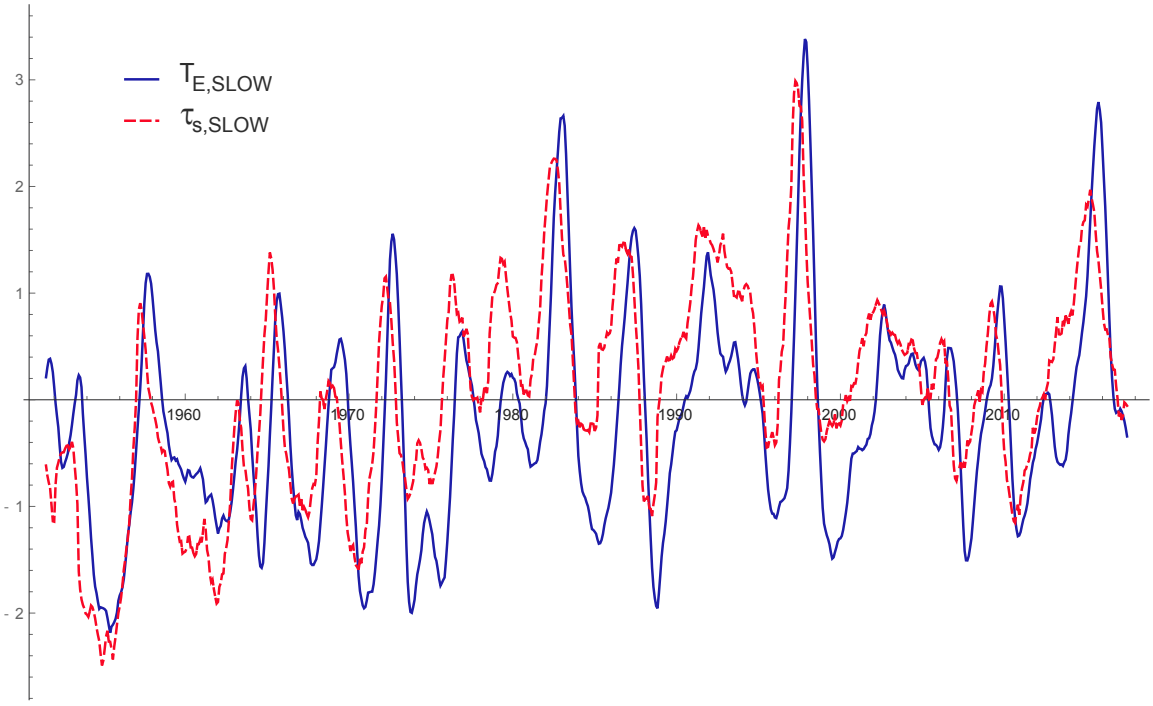

.

Figure A2. Plot of the 13 months averaged NINO3 data (blues solid line) and of the 13 months averaged wind stress anomaly (dashed red line). Quantities are normalized by their respective standard deviations. The NINO3 data are from [39], while the wind stress is proportional to the square of the wind velocity, where the wind data are from [25]. The wind stress has been averaged on the equatorial strip defined by (5S-5N)x(120W-180W)

order moments of the ROM converge to a finite value for $t \to \infty$. It is not difficult to check that the same constraint ensures that also the solution of the FPE of Eq. (17) converges, for $t \to \infty$, to a finite (normalizable) stationary PDF. Thus, under the assumption that $\mu > 3$, from Eq. (C3) we get the stationary PDF given in Eq. (28).

1. Jin, F.F. An Equatorial ocean Recharge Paradigm for ENSO. Part II: A Stripped-Down Coupled Model. *Journal of the Atmospheric Sciences* **1997**, *54*, 830–847.
2. Jin, F.F. An Equatorial ocean Recharge Paradigm for ENSO. Part I: Conceptual Model. *Journal of the Atmospheric Sciences* **1997**, *54*, 811–829.
3. Burgers, G.; Jin, F.F.; van Oldenborgh, G.J. The simplest ENSO recharge oscillator. *Geophysical Research Letters* **2005**, *32*, L13706.
4. Capotondi, A.; Wittenberg, A.; Masina, S. Spatial and temporal structure of Tropical Pacific interannual variability in 20th century coupled simulations. *ocean Modelling* **2006**, *15*, 274 – 298. oceanic results from a new generation of coupled climate models.
5. Jin, F.F.; Lin, L.; Timmermann, A.; Zhao, J. Ensemble-mean dynamics of the ENSO recharge oscillator under state-dependent stochastic forcing. *Geophysical Research Letters* **2007**, *34*, L03807. L03807.
6. Levine, A.F.Z.; Jin, F.F. Noise-Induced Instability in the ENSO Recharge Oscillator. *Journal of the Atmospheric Sciences* **2010**, *67*, 529–542.
7. Ren, H.L.; Jin, F.F. Recharge Oscillator Mechanisms in Two Types of ENSO. *Journal of Climate* **2013**, *26*, 6506–6523, [https://doi.org/10.1175/JCLI-D-12-00601.1].
8. Bianucci, M. Analytical probability density function for the statistics of the ENSO phenomenon: Asymmetry and power law tail. *Geophysical Research Letters* **2016**, *43*, 386–394. 2015GL066772.

Preprints (www.preprints.org) | NOT PEER-REVIEWED | Posted: 13 September 2018 doi:10.20944/preprints201809.0239.v1

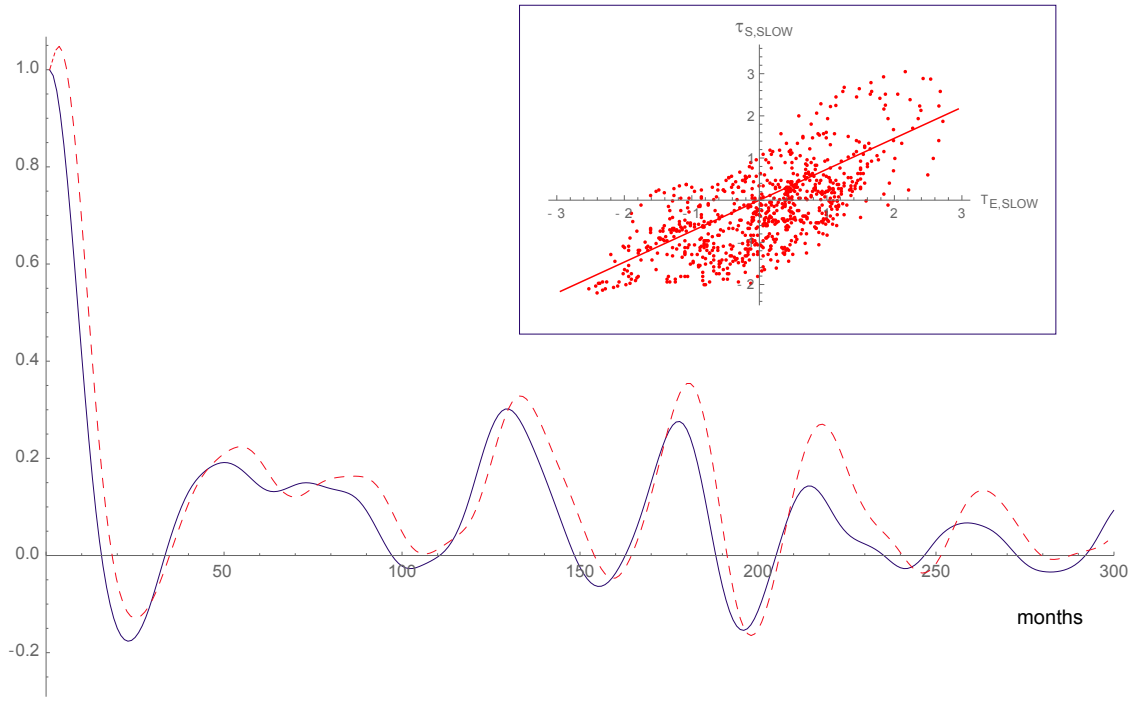

Figure A3. Blue solid line: normalized auto-correlation of the one year averaged NINO3 index: $\langle T_{E,slow}(0)T_{E,slow}(t)\rangle_s / \langle T_{E,slow}(0)T_{E,slow}(0)\rangle_s$. Red-dashed line: cross correlation between the $\tau_{s,slow}$ and $T_{E,slow}$, normalized with the initial value: $\langle \tau_{s,slow}(0)T_{E,slow}(t)\rangle_s / \langle \tau_{s,slow}(0)T_{E,slow}(0)\rangle_s$. We can see that they are very similar to each other. Insert: $\tau_{s,slow}$ vs $T_{E,slow}$ (red dots). Data from http://www.cpc.ncep.noaa.gov/data/indices (NINO3) and [25] (wind).

9. Battisti, D.S.; Hirst, A.C. Interannual variability in a tropical atmosphere-ocean model: influence of the basic state, ocean geometry and nonlinearity. *Journal of the Atmospheric Sciences* **1989**, *46*, 1687–1712.
10. Mantua, N.J.; Battisti, D.S. Evidence for the Delayed Oscillator Mechanism for ENSO: The "Observed" oceanic Kelvin Mode in the Far Western Pacific. *Journal of Physical oceanography* **1994**, *24*, 691–699, [http://dx.doi.org/10.1175/1520-0485(1994)024<0691:EFTDOM>2.0.CO;2].
11. Sardeshmukh, P.D.; Penland, C. Understanding the distinctively skewed and heavy tailed character of atmospheric and oceanic probability distributions. *Chaos* **2015**, *25*, –.
12. Sardeshmukh, P.D.; Sura, P. Reconciling Non-Gaussian Climate Statistics with Linear Dynamics. *Journal of Climate* **2009**, *22*, 1193–1207, [http://dx.doi.org/10.1175/2008JCLI2358.1].
13. Sura, P.; Sardeshmukh, P.D. A global view of air-sea thermal coupling and related non-Gaussian {SST} variability. *Atmospheric Research* **2009**, *94*, 140 – 149. ocean-Atmosphere Coupling.
14. Sardeshmukh, P.D.; Compo, G.P.; Penland, C. Need for Caution in Interpreting Extreme Weather Statistics. *Journal of Climate* **2015**, *28*, 9166–9187, [https://doi.org/10.1175/JCLI-D-15-0020.1].
15. Penland, C.; Sardeshmukh, P.D. Alternative interpretations of power-law distributions found in nature. *Chaos: An Interdisciplinary Journal of Nonlinear Science* **2012**, *22*, 023119, [http://dx.doi.org/10.1063/1.4706504].
16. Khas'minskii, R. A Limit Theorem for the Solutions of Differential Equations with Random Right-Hand Sides. *Theory of Probability & Its Applications* **1966**, *11*, 390–406, [https://doi.org/10.1137/1111038].
17. Gallavotti, G.; Cohen, E.G.D. Dynamical ensembles in stationary states. *Journal of Statistical Physics* **1995**, *80*, 931–970.
18. Gallavotti, G.; Cohen, E.G.D. Dynamical Ensembles in Nonequilibrium Statistical Mechanics. *Phys. Rev. Lett.* **1995**, *74*, 2694–2697.
19. C., P.G.; W., K. Asymptotic theory of mixing stochastic ordinary differential equations. *Communications on Pure and Applied Mathematics*, *27*, 641–668.
20. Dorfman, J.R. *An Introduction to Chaos in Nonequilibrium Statistical Mechanics*; Cambridge Lecture Notes in Physics, Cambridge University Press, 1999.
21. Philander, S.G.H. The Response of Equatorial oceans to a Relaxation of the Trade Winds. *Journal of Physical oceanography* **1981**, *11*, 176–189, [http://dx.doi.org/10.1175/1520-0485(1981)011<0176:TROEOT>2.0.CO;2].
22. Jin, F.F.; Neelin, J.D. Modes of Interannual Tropical ocean-Atmosphere Interaction—a Unified View. Part I: Numerical Results. *Journal of the Atmospheric Sciences* **1993**, *50*, 3477–3503, [http://dx.doi.org/10.1175/1520-0469(1993)050<3477:MOITOI>2.0.CO;2].
23. Neelin, J.D.; Jin, F.F. Modes of Interannual Tropical ocean-Atmosphere Interaction—a Unified View. Part II: Analytical Results in the Weak-Coupling Limit. *Journal of the Atmospheric Sciences* **1993**, *50*, 3504–3522, [http://dx.doi.org/10.1175/1520-0469(1993)050<3504:MOITOI>2.0.CO;2].
24. Kim, S.T.; Jin, F.F. An ENSO stability analysis. Part II: results from the twentieth and twenty-first century simulations of the CMIP3 models. *Climate Dynamics* **2011**, *36*, 1609–1627.
25. [https://www.esrl.noaa.gov/psd/data/gridded/data.ncep.reanalysis.derived.surfaceflux.html]
26. Bianucci, M. Ordinary chemical reaction process induced by a unidimensional map. *Phys. Rev. E* **2004**, *70*, 026107–1–12617–6.
27. Wen, C.; Kumar, A.; Xue, Y.; McPhaden, M.J. Changes in Tropical Pacific Thermocline Depth and Their Relationship to ENSO after 1999. *Journal of Climate* **2014**, *27*, 7230–7249, [https://doi.org/10.1175/JCLI-D-13-00518.1].
28. Bianucci, M. Nonconventional fluctuation dissipation process in non-Hamiltonian dynamical systems. *International Journal of Modern Physics B* **2015**, *30*, 1541004, [http://www.worldscientific.com/doi/pdf/10.1142/S0217979215410040].
29. Grigolini, P. The projection approach to the Fokker-Planck equation: applications to phenomenological stochastic equations with coloured noises. In *Noise in Nonlinear Dynamical Systems*; Moss, F.; McClintock, P.V.E., Eds.; Cambridge University Press: Cambridge, England, 1989; Vol. 1, chapter 5, p. 161.
30. Bianucci, M.; Grigolini, P. Nonlinear and non Markovian fluctuation-dissipation processes: A Fokker-Planck treatment. *The Journal of Chemical Physics* **1992**, *96*, 6138–6148.
31. Bianucci, M.; Mannella, R.; West, B.J.; Grigolini, P. From dynamics to thermodynamics: Linear response and statistical mechanics. *Phys. Rev. E* **1995**, *51*, 3002–3022.
32. Hayashi, M.; Jin, F.F. Subsurface Nonlinear Dynamical Heating and ENSO Asymmetry. *Geophysical Research Letters*, *44*, 12,427–12,435, [https://agupubs.onlinelibrary.wiley.com/doi/pdf/10.1002/2017GL075771].

33. Kapur, A.; Zhang, C. Multiplicative MJO Forcing of ENSO. *Journal of Climate* **2012**, *25*, 8132–8147, [http://dx.doi.org/10.1175/JCLI-D-11-00609.1].
34. Capotondi, A., Sardeshmukh, P. D. and Ricciardulli, L. The nature of the stochastic wind forcing of ENSO. *Journal of Climate* **2018**, *in press*.
35. Sura, P. On non-Gaussian SST variability in the Gulf Stream and other strong currents. *ocean Dynamics* **2010**, *60*, 155–170.
36. Sura, P. A general perspective of extreme events in weather and climate. *Atmospheric Research* **2011**, *101*, 1 – 21.
37. Frankignoul, C. Sea surface temperature anomalies, planetary waves, and air-sea feedback in the middle latitudes. *Reviews of Geophysics* **1985**, *23*, 357–390.
38. Bianucci, M. On the correspondence between a large class of dynamical systems and stochastic processes described by the generalized Fokker Planck equation with state-dependent diffusion and drift coefficients. *Journal of Statistical Mechanics: Theory and Experiment* **2015**, *2015*, P05016.
39. [http://www.cpc.ncep.noaa.gov/data/indices/]
40. Gardiner, C. *Stochastic Methods. A Handbook for the Natural and Social Sciences*, 4 ed.; Vol. 13, *Springer Series in Synergetics*, Springer-Verlag Berlin Heidelberg, 2009; pp. XVIII, 447.
41. Prasad, P.; Ravindran, R. *Partial Differential Equations*; Wiley Eastern, Delhi and John Wiley & Sons, New York, 1985.
42. [http://iridl.ldeo.columbia.edu/]
43. [http://ds.data.jma.go.jp/tcc/tcc/]
44. Bianucci, M.; Capotondi, A.; Mannella, R.; Merlino, S. Estimate of the average timing for strong El Niño events using the Recharge Oscillator Model with a multiplicative perturbation.
    How often strong events of El Niño occur? Inference insight from the Recharge Oscillator Model with a multiplicative perturbation. Submitted.
45. Gardiner, C. *Stochastic Methods*; Vol. 20, *Springer Series in Synergetics*, Springer-Verlag Berlin Heidelberg, 2009.
46. Wang, M.C.; Uhlenbeck, G.E. On the Theory of the Brownian Motion II. *Rev. Mod. Phys.* **1945**, *17*, 323–342.
47. Siegert, A.J.F. On the First Passage Time probability problem. *Physical Review* **1951**, *81*, 617–623.
48. KAMPEN, N.V. Chapter {VIII} - {THE} FOKKER–PLANCK {EQUATION}. In *Stochastic Processes in Physics and Chemistry (Third Edition)*, Third Edition ed.; KAMPEN, N.V., Ed.; North-Holland Personal Library, Elsevier: Amsterdam, 2007; pp. 193 – 218.
49. Bianucci, M.; Mannella, R.; Fan, X.; Grigolini, P.; West, B.J. Standard fluctuation-dissipation process from a deterministic mapping. *Phys. Rev. E* **1993**, *47*, 1510–1519.
50. Zhang, C.; Gottschalck, J. SST Anomalies of ENSO and the Madden-Julian Oscillation in the Equatorial Pacific. *Journal of Climate* **2002**, *15*, 2429–2445.
51. Li, R.C.Y.; Zhou, W.; Chan, J.C.L.; Huang, P. Asymmetric Modulation of Western North Pacific Cyclogenesis by the Madden-Julian Oscillation under ENSO Conditions. *Journal of Climate* **2012**, *25*, 5374–5385, [http://dx.doi.org/10.1175/JCLI-D-11-00337.1].
52. Zavala-Garay, J.; Zhang, C.; Moore, A.M.; Kleeman, R. The Linear Response of ENSO to the Madden-Julian Oscillation. *Journal of Climate* **2005**, *18*, 2441–2459.
53. Hendon, H.H.; Wheeler, M.C.; Zhang, C. Seasonal Dependence of the MJO-ENSO Relationship. *Journal of Climate* **2007**, *20*, 531–543, [http://dx.doi.org/10.1175/JCLI4003.1].
54. Dijkstra, H.A.; Burgers, G. Fluid dynamics of el Niño variability. *Annual Review of Fluid Mechanics* **2002**, *34*, 531–558, [http://dx.doi.org/10.1146/annurev.fluid.34.090501.144936].
55. Bianucci, M. Large Scale Emerging Properties from Non Hamiltonian Complex Systems. *Entropy* **2017**, *19*.
56. Bianucci, M.; Merlino, S., Non Standard Fluctuation Dissipation Processes in ocean-Atmosphere Interaction and for General Hamiltonian or Non Hamiltonian Phenomena: Analytical Results; Mathematics Research Developments, Nova Science Publisher, 2017.
57. Bianucci, M. Using some results about the Lie evolution of differential operators to obtain the Fokker-Planck equation for non-Hamiltonian dynamical systems of interest. *Journal of Mathematical Physics* **2018**, *59*, 053303, [https://doi.org/10.1063/1.5037656].
58. Carmeli, B.; Nitzan, A. Non-Markovian theory of activated rate processes. I. Formalism. *The Journal of Chemical Physics* **1983**, *79*, 393–404.

 doi:10.20944/preprints201809.0239.v1

59. Bianucci, M.; Grigolini, P.; Palleschi, V. Beyond the linear approximations of the conventional approaches to the theory of chemical relaxation. *The Journal of Chemical Physics* **1990**, *92*, 3427–3441.